International Journal of Refrigeration 178 (2025) 51–70

Contents lists available at ScienceDirect

International Journal of Refrigeration

journal homepage: www.elsevier.com/locate/ijrefrig

INSTITUT INTERNATIONAL DU FROID
INTERNATIONAL INSTITUTE OF REFRIGERATION

A comprehensive variable refrigerant flow heat recovery model for building performance simulation

Aziz Mbaye [a,b,*], Massimo Cimmino [a]

[a] Mechanical engineering, Polytechnique Montréal, Québec, Canada
[b] Hydro-Québec Research Institute, Laboratoire des Technologies de l'Énergie, Shawinigan, Québec, Canada

ARTICLE INFO

Keywords:
Variable refrigerant flow (VRF)
Heat pump
Heat recovery
Modeling and simulation
Controller emulation
Calibration and validation

ABSTRACT

A comprehensive, physics-based, and modular Variable Refrigerant Flow with Heat Recovery (VRF-HR) model is developed for multi-year simulations of large-scale VRF systems. The model is designed to simulate various operational modes, including single-mode (cooling-only, heating-only) and heat recovery mode, across any number of indoor units (IUs), outdoor units (OUs), and compressors. A parameter-estimation procedure leveraging manufacturer data is implemented to calibrate the model, ensuring accurate system representation. A machine learning-based control strategy is introduced to emulate real-world compressor selection for partial load operation. The model is validated using two years of operational data from a large-scale VRF system serving the first floor of the former ASHRAE Headquarters Building in Atlanta, USA, which consists of 22 indoor units, 2 outdoor units, and 8 compressors. Results demonstrate that the manufacturer-tuned model accurately predicts total energy consumption, achieving a relative error of 9.5 %, an NMBE of 6.2 %, and a CVRMSE of 27.2 % over the first year. For the second year, the model achieves a CVRMSE of 25.3 %, an NMBE of 5 %, and a relative error of 7 %, meeting ASHRAE calibration criteria.

1. Introduction

Heating, cooling, and hot water production is an important aspect of building operations that directly impacts occupant comfort. Together, they account for 30 % to 70 % of total building energy consumption (X. Li et al., 2014). In this context, Variable Refrigerant Flow (VRF) systems have emerged as an energy-efficient solution, offering significant energy savings. Studies have shown that VRF systems can reduce energy consumption by up to 13 % compared to water-source heat pumps, 49 % compared to air-source heat pumps, and 62 % compared to variable air volume (VAV) systems (Thornton & Wagner, 2012). Their adoption has expanded rapidly, with a compound annual growth rate (CAGR) of 19 % in the U.S. between 2009 and 2019 (BSRIA, ASHRAE Journal, 2021). VRF systems have the ability to dynamically adjust refrigerant flow through a distribution network to meet the specific needs of each indoor unit (IU). This precision is achieved through the controlled operation of the outdoor unit (OU) compressor and electronically regulated valves distributed across the piping network. Additionally, heat recovery VRF systems offer an advanced solution by enabling simultaneous heating and cooling across different building zones. By redistributing heat between zones, the heat recovery process enhances overall energy efficiency, leading to significant reductions in total energy consumption.

To optimize their performance within a specific building, VRF systems require careful design that accounts for factors such as building layout, thermal load distribution, and the number of IUs. As a result, their effective design and implementation rely heavily on robust modeling and simulation techniques (ASHRAE, 2020). Manufacturers often provide proprietary software to aid in the design process, but these tools can limit flexibility by tying HVAC professionals to a specific brand from the early stages of system design. Addressing these limitations calls for versatile simulation tools capable of accurately evaluating energy consumption and operational efficiency. These tools generally fall into two categories: physics-based models and empirical models, each with distinct strengths and limitations (Lin et al., 2015b).

Empirical equation-fit models have become a widely adopted approach for evaluating VRF system performance (Wan et al., 2020). These models are integrated into many Building Energy Performance Simulation (BEPS) tools, such as EnergyPlus (Raustad, 2013; Zhou et al., 2007), and use performance curve functions based on manufacturer data to represent system behavior in a simplified form. This approach eliminates the need for detailed information about component specifications or control strategies, which manufacturers often withhold, and reduces computational costs, making it ideal for simulating large systems.

* Corresponding author: Polytechnique Montreal, 2500 Chem. de Polytechnique, Montréal, QC H3T 0A3, Canada.
E-mail address: aziz.mbaye@polymtl.ca (A. Mbaye).

https://doi.org/10.1016/j.ijrefrig.2025.06.023
Received 11 March 2025; Received in revised form 19 June 2025; Accepted 22 June 2025
Available online 23 June 2025

Nomenclature

Abbreviation

ASHRAE	American Society of Heating, Refrigerating and Air-Conditioning Engineers
BEPS	Building Energy Performance Simulation
COP	Coefficient of Performance
CR	Combination ratio
CVRMSE	Coefficient of Variation of the Root-Mean-Square Error
DOAS	Dedicated Outdoor Air System
HX	Heat Exchanger
HRU	Heat Recovery Unit
HVAC	Heating, Ventilation, and Air Conditioning
IU	Indoor Unit
NMBE	Normalized Mean Bias Error
NTU	Number of transfer units
OU	Outdoor Unit
VRF	Variable Refrigerant Flow
VRF-HR	Variable Refrigerant Flow with Heat Recovery

Symbols

C	Leakage coefficient
cp	Specific isobaric heat capacity
ΔT	Temperature difference
ε	Effectiveness
η	Efficiency
γ	Isentropic exponent
h	Enthalpy
$\dot{m}$	Mass flowrate
N	Number of compressors
$nCom$	Number of working compressors
p	Pressure
$\dot{q}$	Heat transfer rate
R^2	Coefficient of determination
T	Temperature
UA	Thermal conductance
ν	Specific volume
V	Volume
$\dot{V}$	Volume flow rate
$\dot{W}$	Compressor mechanical work
x	vapor quality
X	Water mass fraction

Subscripts

a	Air
c	Coil
cal	Calibrated
con	Condenser
dp	Dew point
db	Dry bulb
eff	Effective
eva	Evaporator
IU	Indoor Unit
lat	Latent
mes	Measured
nom	Nominal
OU	Outdoor Unit
ref	Refrigerant
sat	Saturated
sen	Sensible
suc	Suction
sup	Superheating
wb	Wet bulb

However, empirical models exhibit accuracy limitations, as studies have shown daily energy use relative errors ranging from 25 % (Sharma & Raustad, 2013) to between 15 % and 45 % (Zhou et al., 2008) when compared to field-test data. Additionally, they show significant deviations from manufacturer data under conditions of low outdoor temperatures and low partial load ratios (Torregrosa-Jaime et al., 2019).

Physics-based models describe VRF systems by applying thermodynamic equations based on first principles, enabling detailed predictions of system performance. These models are available in BEPS tools like EnergyPlus (Hong et al., 2016), TRNSYS (Zhu et al., 2013) and Modelica (Dong et al., 2017a). However, their implementation depends key input parameters including evaporator superheating and condenser subcooling (Hong et al., 2016), compressor volumetric and isentropic efficiency (Dong et al., 2017b), and heat exchanger and expansion valve areas (Zhu et al., 2013), which are not always readily available. While effective for designing control strategies and analyzing smaller systems, the computational cost of physics-based models often restricts their application to setups with limited IUs (Wu et al., 2005). To address scalability issues, recent advancements have focused on modular and component-based approaches, improving their adaptability to different system sizes and configurations. More generalized frameworks that accommodate various layouts have also been developed (Sun et al., 2017).

The application of parameter estimation techniques has significantly addressed gaps in data availability, allowing models to more closely replicate real-world conditions (Kim et al., 2018; Pachano et al., 2022; Yun & Song, 2017). However, their applicability in designing VRF systems presents challenges due to the need for onsite data collection. To address this limitation, recent developments have focused on leveraging manufacturer data for parameter estimation. Oh & Kim (2024) proposed a calibrated performance estimation model (PEM) that integrates manufacturer performance data with minimal experimental input. This machine-learning-based approach achieved an R^2 greater than 0.9 and RMSE below 0.2 under dynamic operating conditions, outperforming traditional equation-fit methods. Mbaye & Cimmino (2023) introduced a physics-based VRF model that relies exclusively on manufacturer data for both parameter estimation and a data-driven control strategy. This approach emulates real-world operational behavior without requiring additional experimental data. Validation results over a two-month cooling period demonstrated its accuracy in predicting energy consumption, with a relative error of 1 %, a normalized mean bias error (NMBE) of 1.6 %, and a coefficient of variation of the root mean square error (CVRMSE) of 16.7 %. Further improvements were observed when incorporating actual VRF data. A comparison between controllers tuned on manufacturer data and on monitored data over a two-week period showed that the measurement-tuned controller achieved better accuracy, with a CVRMSE of 10.6 % and an NMBE of -0.4 %, compared to 14.6 % and 5.9 % for the data-tuned controller.

Heat recovery is one of the most notable features of VRF systems, especially in large buildings with diverse thermal loads across zones and during off-peak seasons, such as spring and fall (Zhang et al., 2018). Despite its significance, heat recovery mode remains underexplored in the literature, as it accounts for only 27.3 % of the existing studies in VRF systems (Wang et al., 2024). Consequently, there is limited tools validated for such operations. For instance, the equation-fit VRF heat recovery (VRF-HR) model implemented in EnergyPlus includes performance curve functions to predict system capacity and power during heat recovery. However, due to the lack of manufacturer-provided performance data specific to heat recovery mode, these models rely on approximations, typically applying a constant correction factor to

single-mode performance data. Zhang et al. (2018) addressed this issue by introducing a more physics-based model capable of simulating refrigerant loop performance and incorporating the dynamics of additional operational parameters. While this represents a step forward, such physics-based models require detailed unit-specific data that are often unavailable for commercial systems and operational data that cannot be accessed during the design stage. These limitations continue to hinder the development of accurate and practical VRF heat recovery models, which remain a critical research area for optimizing system performance under dynamic building loads.

The limited exploration of heat recovery operation in the literature is also reflected in the scarcity of validation studies, particularly for systems with a large number of IUs. Most existing studies focus on small-scale systems, highlighting the need for further research on larger installations. Zhang et al. (2018) validated their proposed VRF-HR model using laboratory testbeds consisting of a single OU and two IUs. Their findings showed a coefficient of variation of the root mean square error (CVRMSE) of 2.8 % for cooling mode, 6.9 % for heating mode, and 9.5 % for heat recovery mode when comparing simulated and measured total system power consumption. Lin et al. (2016) aimed to enhance the VRF-HR model in EnergyPlus to better simulate simultaneous space heating, cooling, and water heating. Their approach introduced a new IU model for water heating (WH) and incorporated a thermodynamic model that considers key operational control parameters such as condensing and evaporating temperatures, subcooling, superheat, and suction pressure drop. Validation of their improved model was performed against data collected on a VRF-HR system installed in an office building consisting of two OUs, seven IUs, and one WH unit (Lin et al., 2015a). The results demonstrated a significant improvement in simulation accuracy, with the proposed model achieving a CVRMSE of 10 % compared to 37.4 % for the standard EnergyPlus model. To further understand VRF-HR operation, Hunt et al. (2012) conducted detailed laboratory testing of a VRF-HR system, which included one OU and four IUs, across various operational modes. Their study investigated different values of combination ratio (CR) by varying load conditions while keeping the number of active IUs constant. The system was tested in heating-dominant, balanced, and cooling-dominant modes, with IU return air temperatures set at 21 °C for heating and 26.6 °C for cooling. Results indicated that the VRF-HR system's power consumption remained similar when the number of active IUs was consistent, despite variations in load conditions.

The state-of-the-art review highlights significant challenges in the design and performance evaluation of VRF systems, primarily due to the lack of adequate simulation tools tailored for large commercial buildings. This gap is particularly pronounced for VRF systems operating in heat recovery mode, which offers the highest efficiency potential. Despite its advantages, heat recovery mode remains largely underexplored due to the absence of practically applicable models that have been validated for large-scale commercial applications over an extended period, including peak and shoulder seasons. These barriers limit the ability to accurately assess the full potential of VRF-HR systems in their intended operational environments.

To address these challenges, this study builds upon previous VRF modeling efforts by extending the focus to heat recovery operation. The proposed model adopts a physics-based approach using a simplified vapor compression cycle. Recognizing the challenge of parameter availability, which often limits the applicability of physics-based models, the new model integrates a parameter estimation procedure and a control strategy that leverage manufacturer data. This approach ensures that the model can be effectively calibrated using readily available performance data. The validation of the proposed VRF-HR model is conducted using real-world data from a large-scale system comprising 22 IUs and 2 OUs. The data is sourced from the HVAC system at the former ASHRAE Headquarters Building in Atlanta, USA, covering a two-year operational period that includes diverse load conditions and operational scenarios (Southard et al., 2014a).

2. Methodology

2.1. Modelling approach

A typical VRF system consists of three main components: an OU, multiple IUs distributed throughout the building, and a piping network that circulates refrigerant between these units. Additionally, as presented in Figure 1, the studied system incorporates a Heat Recovery Unit (HRU), which enables simultaneous heating and cooling by redistributing thermal energy across zones. The HRU plays a pivotal role in system operation, directing refrigerant flow to the IUs. It is connected to three dedicated refrigerant pipes, specifically for suction gas, liquid, and discharge gas.

The OU comprises a heat exchanger (HX) and multiple compressors arranged in parallel. The HX facilitates the transfer of thermal energy between the refrigerant and outdoor air, while the compressors ensure the required refrigerant pressure and flow to meet system demands. A centralized controller regulates the entire system, defining the HRU's operational mode and regulating the system's capacity. Each IU is equipped with an expansion device and an HX, facilitating heat exchange between the refrigerant and the zone air. The system operates dynamically based on heating and cooling capacities. For instance, in cooling-dominant mode, the superheated refrigerant exiting the compressors splits into two flows. One flow enters the OU HX, where it condenses and is subsequently expanded through an expansion valve before entering the HRU via the low-pressure liquid pipe. The other flow is directly sent to the HRU via the high-pressure vapor pipe. IUs operating in heating mode receive high-pressure vapor refrigerant from the HRU. The refrigerant condenses within the IU's HX, releasing heat to the zone air. The condensed refrigerant is then expanded through the IU's expansion valve before returning to the HRU via the low-pressure liquid pipe. IUs operating in cooling mode receive low-pressure liquid refrigerant from the HRU. This refrigerant evaporates within the IU by absorbing heat from the zone air to provide cooling. The resulting low-pressure vapor returns to the HRU via the low-pressure vapor pipe, then flows to the compressors to start a new cycle.

The proposed VRF-HR model builds on a simplified vapor compression cycle, as introduced by Jin & Spitler (2002) for water-to-water and water-to-air heat pumps, and incorporates advancements from a previous single-mode VRF model by Mbaye & Cimmino (2023). This approach reduces computational complexity and streamlines parameter estimation by assuming constant superheating, neglecting pressure drops in evaporators and condensers, and focusing on three key thermodynamic states. Compared to distributed parameter methods, this simplification significantly minimizes the number of refrigerant state evaluations required. To expand beyond single-mode operation, the VRF-HR model introduces a framework that accounts for multiple operational modes. The system's key components including IUs, OU, HRU and the controller are represented independently. This modular approach increases flexibility in system configuration and enables adaptability to different operating conditions. To better capture the system complexity, the model also incorporates additional pressure levels and refrigerant states. These enhancements allow for a more accurate representation of heat recovery operations.

2.2. System configuration and operation

The operation of a VRF-HR system can be categorized into two primary states: single mode, where the system operates exclusively in either heating or cooling, and heat recovery mode, where the system simultaneously provides both heating and cooling. These states are further divided into five distinct operational modes, as represented on Figure 2, based on the status of the IUs and their respective heating and cooling load requirements:

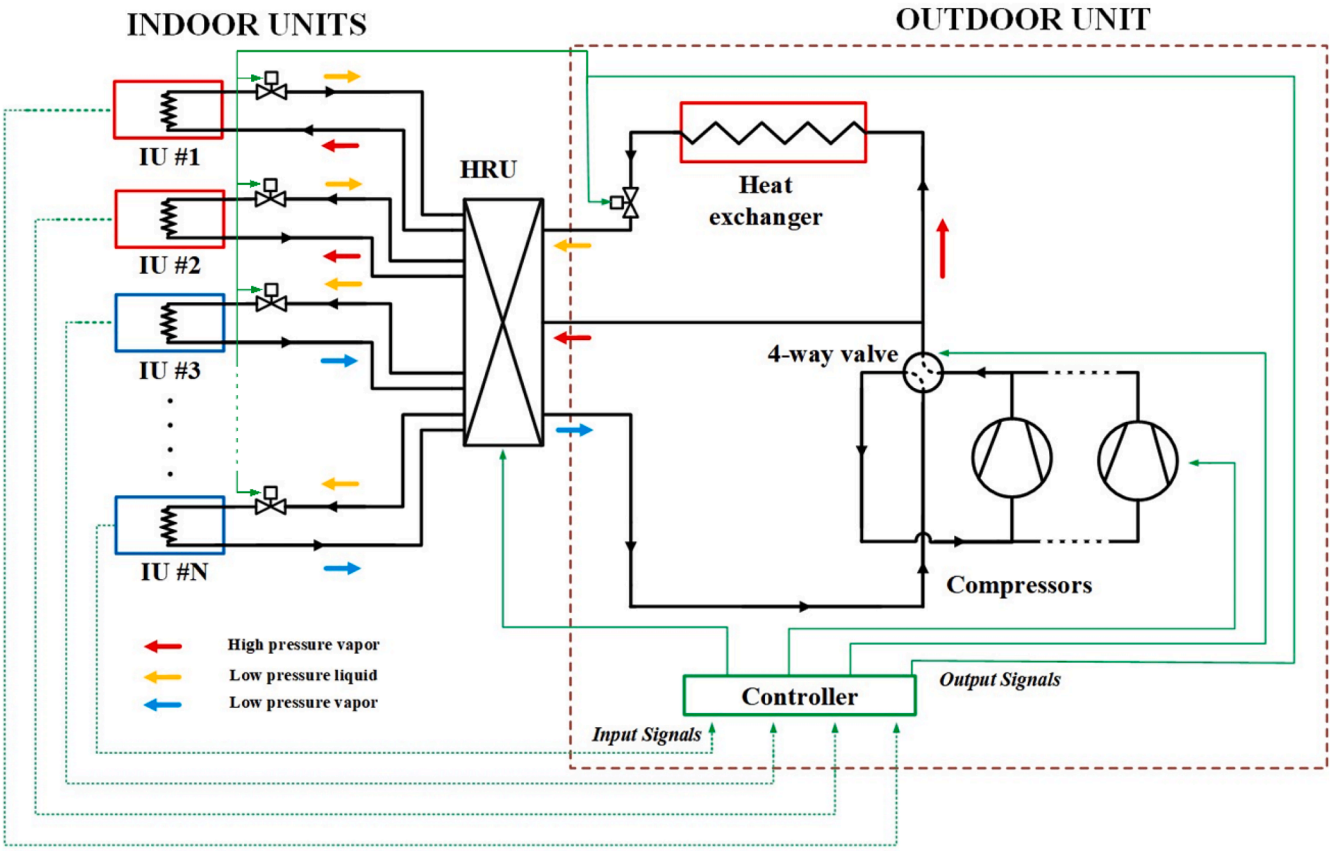

Fig. 1. Schematic diagram of the studied VRF system in cooling-dominant mode.

(1) Heating only mode: All IUs require heating, with no cooling demand present. The OU functions as an evaporator, while all IUs operate as condensers.
(2) Cooling only mode: All IUs require cooling, with no heating demand present. The OU functions as a condenser, while all IUs operate as evaporators.
(3) Heating dominant mode: Simultaneous heating and cooling are required, but the combined cooling capacity and compressor work are less than the total heating capacity. To satisfy the heating requirements, the OU operates as an evaporator. During winter, significant temperature differences may occur between the IUs operating in cooling mode (i.e. functioning as evaporators) and the OU, due to the colder outdoor conditions. To accurately represent these differences, the thermodynamic cycle incorporates distinct evaporating refrigerant temperatures for the IUs and the OU, ensuring the model reflects their unique operational characteristics.
(4) Cooling dominant mode: Simultaneous heating and cooling are required, but the cooling capacity exceeds the heating capacity. The OU operates as a condenser to meet the cooling requirements.
(5) Balanced mode: Both heating and cooling loads are present, and the total heating capacity exceeds the cooling capacity but remains less than the sum of the cooling capacity and compressor work. The OU alternates between functioning as an evaporator or a condenser to maintain energy balance. For systems with multiple HX in the OU, one half operates as an evaporator, and the other half functions as a condenser. Similar to the heating dominant mode, separate evaporator temperatures are considered for the IUs and OU.

3. VRF heat recovery model

3.1. Heat exchanger

Considering an air-to-air VRF system, the IU is comparable to an air-refrigerant HX operating at a constant refrigerant temperature. The HX model is described using the enthalpy potential method (McElgin & Wiley, 1940) and the coil sensible and latent heat transfer rates are evaluated by applying the ε-NTU method. As presented in Mbaye & Cimmino (2023), the IU model has 2 parameters: the heat transfer coefficient between the moist air and the coil surface (UA_c) and the heat transfer coefficient between the refrigerant and the coil inside surface (UA_{ref}).

The coil heat transfer is modelled using the enthalpy potential method, which splits the total heat transfer rate ($\dot{q}$) into sensible heat transfer ($\dot{q}_{sen}$) and latent heat transfer ($\dot{q}_{lat}$). Sensible heat transfer is determined by the temperature difference between the air stream and the coil's effective surface temperature ($T_{c,eff}$) using the ε-NTU method:

$$\dot{q}_{sen} = \varepsilon_{sen}\dot{m}_a c_{p,a}\left(T_{db,a} - T_{c,eff}\right) \quad (1)$$

$$\varepsilon_{sen} = 1 - e^{(-NTU_{sen})} \quad (2)$$

$$NTU_{sen} = UA_c/\dot{m}_a c_{p,a} \quad (3)$$

where $\dot{m}_a$ is the air mass flow rate, $c_{p,a}$ is the specific heat capacity of moist air, and $T_{db,a}$ is the inlet air dry bulb temperature. The effective surface temperature defines the coil's surface condition. If $T_{c,eff}$ is below the dew point temperature ($T_{dp,a}$), condensation occurs, resulting in a wet coil regime. For these conditions, $T_{c,eff}$ is inferred by solving a nonlinear equation that relates the total heat transfer ($\dot{q}$) and the enthalpy difference between the air stream and coil surface:

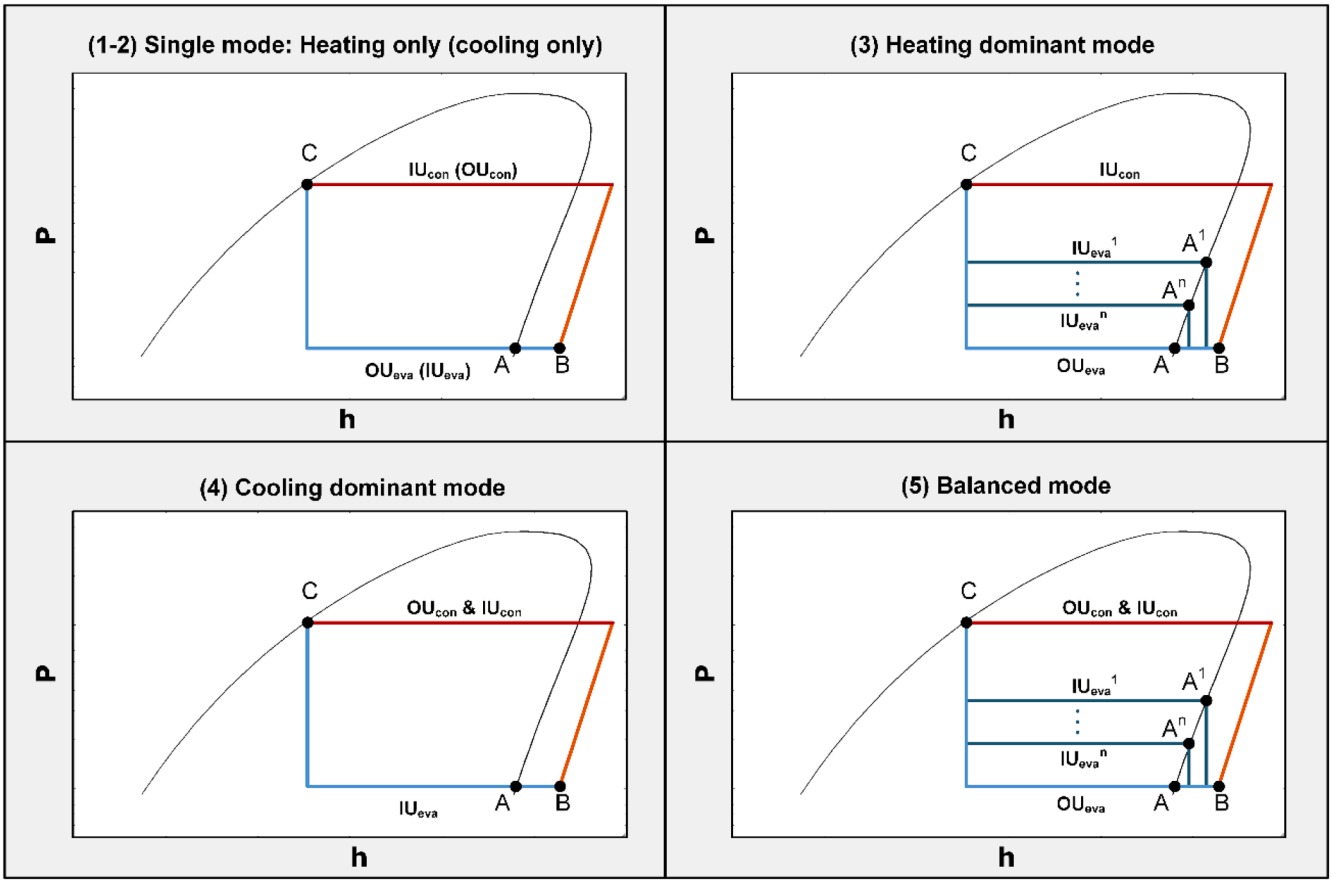

Fig. 2. P-h diagram of the VRF-HR operation modes.

$$\dot{q} = \varepsilon_{sen}\dot{m}_a\left(h_a - h_{a,c,eff}\right) \tag{4}$$

$$h_{a,c,eff} = f\left(T_{c,eff}, X_{a,sat}\big|_{T=T_{c,eff}}\right) \tag{5}$$

where h_a is the inlet air enthalpy, $h_{a,c,eff}$ is the specific enthalpy of saturated air at $T_{c,eff}$ and its corresponding humidity ratio ($X_{a,sat}$) and f refers to a thermodynamic state function.

The total heat transfer rate is also evaluated between the air stream and the refrigerant using a global heat transfer coefficient:

$$\dot{q} = \varepsilon\dot{m}_a\left(h_a - h_{a,ref}\right) \tag{6}$$

$$\varepsilon = 1 - e^{(-NTU)} \tag{7}$$

$$NTU = UA/\dot{m}_a c_{p,a} \tag{8}$$

$$UA = \left(\frac{1}{UA_c} + \frac{c_{p,a,c}}{c_{p,a}}\frac{1}{UA_{ref}}\right)^{-1} \tag{9}$$

The effective specific isobaric heat capacity of air that considers water condensation ($c_{p,a,c}$) and the enthalpy of moist air at the refrigerant temperature ($h_{a,ref}$) are evaluated as follows:

$$h_{a,ref} = f\left(T_{ref}, X_{a,sat}\big|_{T=T_{ref}}\right) \tag{10}$$

$$c_{p,a,c} = \left.\frac{dh_{a,s}}{dT}\right|_{T=T_{ref}} \approx \frac{h_{a,s}\big|_{T_{ref}+\Delta T} - h_{a,s}\big|_{T_{ref}}}{\Delta T} \tag{11}$$

where T_{ref} is the refrigerant temperature, $h_{a,s}$ is the enthalpy of saturated air. A temperature difference (ΔT) of 0.1 °C is considered for the finite differences approximation of the saturated air enthalpy derivative. The latent heat transfer ($\dot{q}_{lat}$) is calculated as the difference between total and sensible heat transfer rates:

$$\dot{q}_{lat} = \dot{q} - \dot{q}_{sen} \tag{12}$$

In heating mode, when the coil operates as a condenser, $T_{c,eff}$ is always above $T_{dp,\,a}$, resulting in a dry coil with no latent heat transfer ($\dot{q}_{lat}$=0). The heat transfer calculations remain the same, but air properties are evaluated as:

$$h_{a,c,eff} = f\left(T_{c,eff}, X_a\right) \tag{13}$$

$$h_{a,ref} = f\left(T_{ref}, X_a\right) \tag{14}$$

$$c_{p,a,c} = c_{p,a} \tag{15}$$

where X_a is the mass fraction of water in the air mixture at the inlet air conditions.

3.2. Compressor

The VRF system is assumed to utilize a scroll compressor, with its mechanical work modeled as a two-stage process (Winandy et al., 2002): (1) an isentropic compression at the built-in volume ratio and (2) an isochoric compression to the discharge pressure. Following the formulation of Jin (2002), the theoretical work of the compressor ($\dot{W}_t$) is calculated using the evaporating and condensing pressures (p_{eva}, p_{con}), nominal suction volume flow rate ($\dot{V}_{nom}$), isentropic exponent (γ), and built-in volume ratio (V_r):

$$\dot{W}_t = \frac{\gamma}{\gamma - 1}p_{eva}\dot{V}_{nom}\left(\frac{\gamma}{\gamma - 1}\frac{p_{con}}{p_{eva}V_r} + \frac{1}{\gamma}p_r^{\frac{\gamma}{\gamma-1}} - 1\right) \tag{16}$$

where $p_r = V_r^{\gamma}$ is the built-in pressure ratio. The isentropic exponent ($\gamma = c_p/c_v$) is assumed constant and is evaluated at the compressor suction conditions (i.e., at $T = T_{eva} + \Delta T_{sup}$ and $p = p_{eva}$). This simplification is widely adopted in compressor modeling studies, including by Jin & Spitler (2002). As an illustrative example, for an isentropic compression process, a sample calculation for R410A shows that γ varies from 1.116 at suction conditions (T_{eva} = -5 °C, ΔT_{sup} = 5 °C) to 1.051 at a discharge temperature of 40 °C, representing a relative variation of approximately 5.8 %. The actual compressor power input ($\dot{W}$) accounts for electro-mechanical efficiency (η) and constant power losses ($\dot{W}_{loss}$):

$$\dot{W} = \frac{\dot{W}_t}{\eta} + \dot{W}_{loss} \tag{17}$$

Refrigerant mass flow rate ($\dot{m}_{ref}$) is calculated by considering leakage effects, as described by Chen et al. (2000):

$$\dot{m}_{ref} = \frac{\dot{V}_{nom}}{\nu_{suc}} - C\frac{p_{con}}{p_{eva}} \tag{18}$$

where, ν_{suc} is the refrigerant's specific volume at the compressor suction and C is the leakage coefficient.

3.3. Heat recovery unit

In VRF-HR systems, the HRU facilitates simultaneous heating and cooling. The HRU achieves this by monitoring zone temperatures and dynamically adjusting refrigerant flow to meet the specific heating and cooling demands of different zones. For VRF systems equipped with multiple compressors, the total refrigerant mass flow rate ($\dot{m}_{ref,VRF}$) is calculated as the sum of the individual mass flow rates of each compressor:

$$\dot{m}_{ref,VRF} = \sum_i \left(\frac{\dot{V}_{nom}^{(i)}}{\nu_{suc}} - C^{(i)}\frac{p_{con}}{p_{eva}} \right) \tag{19}$$

where i denotes the compressor index.

In addition to regulating refrigerant flow, the HRU interacts with the VRF control system to determine the appropriate operating mode based on the IUs operation modes and capacities. To capture its behavior, the HRU model is designed to determine the refrigerant flow distribution among the IUs and the OU, as well as to establish the total energy balance under various load conditions.

The HRU model is structured around the simplified vapor compression cycles and operates in five distinct modes: two single modes (heating only and cooling only) and three heat recovery modes. Each mode reflects a specific combination of heating and cooling loads, allowing the system to adapt to varying operational scenarios.

3.3.1. Heating only mode

In single mode, the VRF-HR system operates similarly to a conventional heat pump, where all IUs share the same refrigerant temperature. In heating only mode, all IUs act as condensers since there is no cooling load. The condensing temperature is set by the IU with the highest setpoint temperature. The total refrigerant mass flow rate is assumed to be distributed in an idealized manner among the indoor units (IUs), proportionally to their nominal capacities. This distribution varies during operation depending on which IUs are active, but it does not adapt dynamically to real-time control signals such as setpoint changes or valve positions. The refrigerant flow rate to each IU is given by:

$$\dot{m}_{ref,IU}^{(i)} = \dot{m}_{ref,VRF}\frac{\sigma^{(i)}\dot{q}_{nom,IU}^{(i)}}{\sum_i \sigma^{(i)}\dot{q}_{nom,IU}^{(i)}} \tag{20}$$

where $\dot{m}_{ref,IU}^{(i)}$ and $\dot{q}_{nom,IU}^{(i)}$ are respectively the refrigerant mass flowrate and the nominal capacities of the i-th IU and $\sigma^{(i)}$ is operation signal, which is equal to 1 when the IU is on and 0 when it is off. This assumption simplifies the control logic and allows the model to ensure consistent energy balance across zones with different thermal loads.

The total energy balance is expressed as follows:

$$\dot{W}_{VRF} = \sum_i \frac{\dot{W}_t^{(i)}}{\eta^{(i)}} + \dot{W}_{loss}^{(i)} \tag{21}$$

$$\dot{q}_{eva} = \dot{m}_{ref,VRF}(h_A - h_C) \tag{22}$$

$$h_A = f(p_{eva}, x = 1) \tag{23}$$

$$h_C = f(p_{con}, x = 0) \tag{24}$$

$$\dot{q}_{con} = -(\dot{q}_{eva} + \dot{W}_{VRF}) \tag{25}$$

$$\dot{q}_{eva} = \dot{q}_{OU} \tag{26}$$

$$\dot{q}_{con} = \sum_i \dot{q}_{IU}^{(i)} \tag{27}$$

where i represents the compressor index, $\dot{q}_{eva}$ is the total evaporator heat transfer rate, $\dot{q}_{con}$ is the total condenser heat transfer rate, h_A is the refrigerant enthalpy at point A, h_C is the refrigerant enthalpy at point C, x is the vapor quality, $\dot{q}_{OU}$ is the heat transfer rate of the OU and $\dot{q}_{IU}^{(i)}$ is the heat transfer rate of the i-th IU.

3.3.2. Cooling only mode

In cooling only mode, all IUs operate as evaporators, with the IU set to the lowest temperature setpoint determining the evaporating temperature for the system. The refrigerant flow distribution and total energy balance are calculated using the same equations as in heating only mode. The primary difference from heating only mode lies in the heat transfer rates for the evaporator and condenser, which are evaluated as follows:

$$\dot{q}_{eva} = \sum_i \dot{q}_{IU}^{(i)} \tag{28}$$

$$\dot{q}_{con} = \dot{q}_{OU} \tag{29}$$

3.3.3. Heating dominant mode

The heating dominant mode represents a scenario where both heating and cooling loads are present, but the combined total heating capacity across all zones exceeds the total cooling capacity plus the compressor work. As illustrated in the pressure-enthalpy diagram (Figure 2 (3)), the indoor unit evaporators (IU_{eva}) operate at varying evaporating temperatures depending on the specific zone loads and setpoint temperatures. Each evaporator's temperature is determined by its corresponding operational conditions. Conversely, the evaporating temperature of the outdoor unit evaporator (OU_{eva}) is influenced directly by the outdoor air temperature. In reality, VRF systems operate with a common evaporating pressure, meaning that all IU_{eva} share the same evaporating temperature, provided that pressure drops in the refrigerant piping are negligible. Capacity modulation at the zone level is achieved by adjusting the refrigerant mass flow rate through each unit. In the present model, however, we assume an idealized flow distribution where the refrigerant mass flow rate allocated to each evaporator remains constant throughout operation and is proportional to its nominal capacity. This assumption results in varying evaporating temperatures across the IU_{eva} and OU_{eva}, enabling the model to reflect capacity variations driven by differences in zone temperatures and outdoor air conditions. This differentiation is essential to maintaining the overall energy balance of the system, particularly under operating scenarios with significant temperature disparities between indoor and outdoor evaporators. As a result of this assumption, the compressor suction pressure is defined by the lowest evaporating temperature

among all the evaporators, as the refrigerant from each evaporator is mixed before entering the compressor. It is assumed that the refrigerant exits each evaporator in a saturated state, and the mixed refrigerant enters the compressor with a constant degree of superheating. As a result, additional refrigerant states must be evaluated to account for the distinct operating conditions of each IU. Specifically, the refrigerant enthalpy at the outlet of each IU_{eva}, corresponding to the saturated vapor enthalpy at each point A^i (h_{A^i}), is required for accurate modeling of this mode.

The refrigerant flow distribution among the evaporators and condensers is also determined based on their nominal capacities. For the IU_{eva} and the OU_{eva}, the flow rates are calculated as follows:

$$\dot{m}^{(i)}_{ref,IU_{eva}} = \dot{m}_{ref,VRF}\frac{\dot{q}^{(i)}_{nom,IU_{eva}}}{\sum_i \dot{q}^{(i)}_{nom,IU_{eva}} + \dot{q}_{nom,OU_{eva}}} \tag{30}$$

$$\dot{m}_{ref,OU_{eva}} = \dot{m}_{ref,VRF}\frac{\dot{q}_{nom,OU_{eva}}}{\sum_i \dot{q}^{(i)}_{nom,IU_{eva}} + \dot{q}_{nom,OU_{eva}}} \tag{31}$$

For the indoor unit condensers (IU_{con}), the refrigerant flow is distributed as:

$$\dot{m}^{(i)}_{ref,IU_{con}} = \dot{m}_{ref,VRF}\frac{\dot{q}^{(i)}_{nom,IU_{con}}}{\sum_i \dot{q}^{(i)}_{nom,IU_{con}}} \tag{32}$$

The total energy balance for this mode (as described in Equation 17) remains valid, where the total evaporator and condenser heat transfer rates are given by:

$$\dot{q}_{eva} = \sum_i \dot{m}^{(i)}_{ref,IU_{eva}}(h_{A^i} - h_C) + \dot{m}_{ref,OU_{eva}}(h_A - h_C) \tag{33}$$

$$\dot{q}_{con} = \sum_i \dot{q}^{(i)}_{IU_{con}} \tag{34}$$

3.3.4. Cooling dominant mode

The cooling dominant mode occurs when both heating and cooling demands are present, but the total cooling capacity across all zones surpasses the combined total of the heating capacity. In this mode, the IUs with cooling demands operate as evaporators (IU_{eva}), all sharing the same evaporating temperature. Conversely, the IUs serving heating zones and the OU function as condensers (IU_{con} *and* OU_{con}). Given the relatively small temperature difference between the refrigerant condensation temperature in the heating zone indoor units and the outdoor unit, and the likelihood of the outdoor temperature being higher than the heating zone temperatures, it is assumed that both IU_{con} and OU_{con} have the same condensing temperature.

The refrigerant flow rates for the IU_{eva}, IU_{con} and OU_{con} are determined as follows:

$$\dot{m}^{(i)}_{ref,IU_{eva}} = \dot{m}_{ref,VRF}\frac{\dot{q}^{(i)}_{nom,IU_{eva}}}{\sum_i \dot{q}^{(i)}_{nom,IU_{eva}}} \tag{35}$$

$$\dot{m}^{(i)}_{ref,IU_{con}} = \dot{m}_{ref,VRF}\frac{\dot{q}^{(i)}_{nom,IU_{con}}}{\sum_i \dot{q}^{(i)}_{nom,IU_{con}} + \dot{q}_{nom,OU_{con}}} \tag{36}$$

$$\dot{m}_{ref,OU_{con}} = \dot{m}_{ref,VRF}\frac{\dot{q}_{nom,OU_{con}}}{\sum_i \dot{q}^{(i)}_{nom,IU_{con}} + \dot{q}_{nom,OU_{con}}} \tag{37}$$

The total energy balance equations, as defined earlier (Equations 16 and 17), are still valid in this mode. The total heat transfer rates for the evaporators and condensers are expressed as follows:

$$\dot{q}_{eva} = \sum_i \dot{q}^{(i)}_{IU_{eva}} \tag{38}$$

$$\dot{q}_{con} = \sum_i \dot{q}^{(i)}_{IU_{con}} + \dot{q}_{OU_{con}} \tag{39}$$

3.3.5. Balanced mode

The balanced mode occurs when the total heating and cooling capacities are approximately equal within a certain range. This mode represents a less obvious form of heat recovery operation and is one of the least documented in the literature. Its operational characteristics, including the behavior of the OU, are often dependent on the specific commercial product and the configuration defined by the system's native controller.

In some systems, the outdoor unit heat exchanger alternates between functioning as a condenser and an evaporator to balance the heat exchange between the IUs. In scenarios where the cooling and heating capacities are perfectly balanced, the OU HX may even shut down completely, as noted by Y. M. Li & Wu (2010). For systems with multiple OUs or OUs featuring multiple HX, the balanced mode can operate differently. In these configurations, part of the outdoor HX act as condensers, while the remaining HX function as evaporators, as described by Zhang et al. (2018). This operational flexibility enables balanced mode to effectively adapt to varying load conditions. To optimize the OU transition between evaporator and condenser operation, Dong, Li, House, et al. (2017) proposed a mode-switching strategy for the OU HX based on the difference between the inlet and outlet outdoor air temperatures. Their method utilizes this temperature differential, normalized by the dimensionless fan speed, to trigger the switching process. However, while this strategy is useful for control purposes, it is less applicable for system design, as the specific decision thresholds required for commercial units are not readily available.

The presented model defines the operational range for the balanced mode based on the nominal capacities of the IU evaporators and condensers, as well as the VRF-HR nominal power consumption ($\dot{W}_{nom,VRF}$). The balanced mode is activated when the following condition is satisfied:

$$0 \le \sum_i \dot{q}^{(i)}_{nom,IU_{con}} - \sum_i \dot{q}^{(i)}_{nom,IU_{eva}} < \dot{W}_{nom,VRF} \tag{40}$$

Here, $\sum_i \dot{q}^{(i)}_{nom,IU_{con}}$ represents the total nominal heating capacity of the IU condensers, and $\sum_i \dot{q}^{(i)}_{nom,IU_{eva}}$ represents the total nominal cooling capacity of the IU evaporators. The model accommodates both approaches for the OU operation. For systems equipped with multiple HX in the OU, one half of the HX operates as an evaporator, while the other half functions as a condenser to balance the thermal loads. For systems featuring only a single HX in the OU, the HX operates exclusively as an evaporator during balanced mode.

The refrigerant flow distribution among the evaporators and condensers is similarly to the heating dominant mode:

$$\dot{m}^{(i)}_{ref,IU_{eva}} = \dot{m}_{ref,VRF}\frac{\dot{q}^{(i)}_{nom,IU_{eva}}}{\sum_i \dot{q}^{(i)}_{nom,IU_{eva}} + \dot{q}_{nom,OU_{eva}}} \tag{41}$$

$$\dot{m}_{ref,OU_{eva}} = \dot{m}_{ref,VRF}\frac{\dot{q}_{nom,OU_{eva}}}{\sum_i \dot{q}^{(i)}_{nom,IU_{eva}} + \dot{q}_{nom,OU_{eva}}} \tag{42}$$

$$\dot{m}^{(i)}_{ref,IU_{con}} = \dot{m}_{ref,VRF}\frac{\dot{q}^{(i)}_{nom,IU_{con}}}{\sum_i \dot{q}^{(i)}_{nom,IU_{con}} + \dot{q}_{nom,OU_{con}}} \tag{43}$$

$$\dot{m}_{ref,OU_{con}} = \dot{m}_{ref,VRF}\frac{\dot{q}_{nom,OU_{con}}}{\sum_i \dot{q}^{(i)}_{nom,IU_{con}} + \dot{q}_{nom,OU_{con}}} \tag{44}$$

The total evaporator and condenser heat transfer rates are given by:

$$\dot{q}_{eva} = \sum_i \dot{m}^{(i)}_{ref,IU_{eva}}(h_{A^i} - h_C) + \dot{m}_{ref,OU_{eva}}(h_A - h_C) \tag{45}$$

$$\dot{q}_{con} = \sum_i \dot{q}^{(i)}_{IU_{con}} + \dot{q}_{OU_{con}} \tag{46}$$

3.4. Model implementation

Building upon the previously developed single-mode VRF model implemented in Modelica using the IBPSA library (Wetter et al., 2015), the VRF-HR model follows the same approach. The IBPSA library offers a robust framework for modeling complex HVAC systems, enabling flexible and scalable simulations. The VRF-HR system is structured by integrating an HRU model with an OU model and multiple IU models, utilizing a vector-based implementation that accommodates configurations with a large number of units.

In the VRF-HR model, the IU represents the HX, while the OU consists of both the HX and one or more scroll compressors. The simulation process remains consistent with the previous single-mode model, involving the resolution of a nonlinear system of equations that captures key component interactions. These interactions are primarily defined by essential refrigerant properties, including the saturation pressures at the condenser (p_{con}) and evaporator (p_{eva}), as well as the total refrigerant mass flow rate ($\dot{m}_{ref,VRF}$).

The VRF-HR system simulation requires various input parameters, such as the dry bulb and wet bulb temperatures, and return air mass flow rate for indoor zones, in addition to outdoor conditions, including temperature, humidity ratio, and air mass flow rate.

4. Model calibration

The calibration of the VRF-HR model involves estimating key parameters for its main components, including the IUs and the OU. These parameters consist of the HX conductance values (UA_c and UA_{ref}) for both the IUs and OU, as well as compressor-specific characteristics ($\dot{V}_{nom}$, V_r, C, η, $\dot{W}_{loss}$ and ΔT_{sup}). For commercial systems, these parameters are identified using a parameter estimation procedure based on manufacturer data. Since VRF-HR systems equipped with multiple single-speed compressors require efficient part-load operation, a dedicated control strategy is necessary to determine the appropriate number of operating compressors based on system capacity. Ideally, controller development would rely on real-world operational data to better capture site-specific characteristics and dynamic behavior. However, when such data is unavailable, the design process can leverage manufacturer performance data to achieve a practical and adaptable control strategy

4.1. Parameter estimation

A parameter estimation procedure was developed for the single-mode VRF model, leveraging manufacturer data to obtain parameters by minimizing the error between simulation results and reference data. A detailed calibration procedure, including cost functions, model inputs, and outputs, as well as guess values selection for the IUs and OU, was presented in Mbaye & Cimmino (2023). This calibration method, classified as a macro parameter estimation approach (Reddy, 2006), evaluates aggregate system performance parameters. However, different parameter sets may be required for heating and cooling operations due to variations in compressor characteristics between the two modes. Furthermore, manufacturer data typically provides performance metrics only for single-mode operations (heating-only and cooling-only). Since the VRF-HR model is intended for both single-mode and heat recovery operation, the initial estimation method needs to be adapted to account for all operating modes.

To address this, the parameter estimation procedure for the VRF-HR model involves calibrating the OU model using manufacturer data for both heating and cooling modes, while the IU model is calibrated using data from cooling mode only. The IU HX model considers both sensible and latent heat transfer, capturing both wet and dry coil regimes. As a result, calibration using cooling mode data provides parameter values applicable to both heating and cooling operations, where the heating mode corresponds to a dry coil regime with only sensible heat transfer.

Regarding compressor parameters, characteristics such as superheating degree (ΔT_{sup}), built-in volume ratio (V_r), and power losses ($\dot{W}_{loss}$) vary between heating and cooling operations. Due to the interdependence of calibration parameters, the OU model is calibrated separately for heating and cooling conditions to obtain distinct parameter sets. The model uses the heating-calibrated parameter set for the following operating modes: heating-only, heating-dominant, and balanced. Conversely, it uses the cooling-calibrated parameter set during cooling-dominant and cooling-only modes. No explicit transition criteria are implemented between the heating and cooling parameter sets. At each simulation timestep, the compressor parameters are selected directly based on the active operation mode signal, which determines whether the heating-calibrated or cooling-calibrated values are applied.

4.2. Control method

4.2.1. Controller design

In the single-mode VRF model, the control strategy is designed to optimize the operation of multiple single-speed compressors to ensure system capacity matches IU demands. This strategy relies on a compressor map, which determines the number of compressors (*nCom*) required under various operating conditions The map is generated by simulating the calibrated VRF model across different configurations and minimizing discrepancies with reference data. When available, system capacity or power consumption data is used; otherwise, values from performance tables serve as a reference. The key parameters influencing the compressor map include IU and OU dry bulb temperatures and the combination ratio (CR), which defines the ratio of the total nominal capacity of active IUs to the OU nominal capacity.

In heat recovery mode, however, both heating and cooling loads exist simultaneously, making it unclear how to define CR consistently across all operational modes. Existing definitions do not account for scenarios where some IUs act as evaporators while others function as condensers. Previous studies, such as Hunt et al. (2012), suggest that in heat recovery mode, system power consumption remains stable when the number of active IUs is constant, regardless of variations in load conditions. This finding motivates a revised definition of CR that prioritizes the number of active IUs rather than their specific loads, ensuring consistency between single-mode and heat recovery operations. This revised CR definition is expressed as follows:

$$CR = \frac{\sum_i \sigma^{(i)} \dot{q}^{(i)}_{nom,IU}}{\dot{q}_{nom,OU}} \tag{47}$$

where $\sigma^{(i)}$ s a binary signal equal to 1 if the i-th IU is active (either in heating or cooling mode), and 0 otherwise. To adapt the compressor control strategy for heat recovery mode, three key modifications are introduced: redefining temperature variables, generating a compressor map for single-mode operation, and establishing compressor selection rules for HR mode.

In HR mode, system capacity is primarily influenced by the evaporator and condenser with the most extreme entering air temperatures. These temperatures are defined as:

$$T_{low} = \min\left(T^{(i)}_{IU_{eva}};\ T^{(j)}_{OU_{eva}}\right) \tag{48}$$

$$T_{high} = \max\left(T^{(i)}_{IU_{con}};\ T^{(j)}_{OU_{con}}\right) \tag{49}$$

where T_{low} represents the lowest return air temperature among all evaporators, and T_{high} represents the highest return air temperature among all condensers.

The VRF-HR compressor map is generated separately for heating-only and cooling-only operations using manufacturer-provided data. This process will result in two distinct values for the number of com-

pressors required: one for heating operation ($nCom_{heating}$) and one for cooling operation ($nCom_{cooling}$).

Since performance data for heat recovery operation is not available, the compressor selection in these modes follows the same approach used in the parameter estimation procedure. Specifically, for heating-only, heating-dominant, and balanced modes, the controller will utilize $nCom_{heating}$, as these modes primarily align with heating conditions. Conversely, for cooling dominant and cooling only modes, the controller will refer to $nCom_{cooling}$.

When actual VRF system data, including heat recovery mode operation, is available, the compressor map is refined by incorporating the operating mode in addition to T_{low}, T_{high} and CR. The map is generated by simulating the calibrated VRF-HR model under various operating conditions, testing all possible combinations of operating mode and number of compressors. The optimal compressor configuration is then determined by selecting the option that minimizes the error between the model's output and measured data.

4.2.2. Controller implementation

The VRF-HR capacity controller is implemented using a machine learning approach, which effectively captures the complex and nonlinear relationships between the operational variables. A decision tree algorithm is used to classify the number of active compressors based on system operating conditions. Decision trees are particularly well-suited for this application due to their ability to generate transparent, human-readable rules, making them ideal for integration into Modelica-based system simulations.

The control strategy can be developed using both manufacturer and field test data to train the decision tree model. To ensure the model's robustness and prevent overfitting, the dataset is split into 80 % for training and 20 % for testing. Additionally, the depth of the decision tree is limited to the number of compressors minus one, ensuring that the learned decision rules align with the actual physical behavior of the system. The input variables for the controller vary depending on the data source used for training. For the manufacturer-tuned controller, which is trained with manufacturer data, the inputs consist of T_{low}, T_{high} and CR. In contrast, the measurement-tuned controller, which is trained using monitored field data, the HRU operation mode, in addition to T_{low}, T_{high} and CR. The performance of the trained controller models is evaluated using standard classification metrics, including accuracy, precision, recall, and F1-score. These metrics provide a comprehensive assessment of the model's capability to predict compressor activation under various operating conditions.

5. Validation

5.1. Description of the Building and VRF-HR System

The former ASHRAE Headquarters Building in Atlanta, USA, serves as the testbed for validating the VRF heat pump model and its control strategy. The building's first floor includes diverse spaces, including office areas, conference rooms, a learning center, computer rooms, and an elevator machine room. These areas are conditioned by 22 ducted IUs of varying capacities, each serving a distinct thermal zone. As illustrated in Figure 3, the IUs are connected to the OUs through an extensive piping network that integrates both three-pipe and two-pipe configurations, with branch selectors directing refrigerant flow based on the specific heating and cooling demands of each zone. The system comprises two outdoor heat recovery units OUs with a combined cooling capacity of 98 kW (49 kW each). Each OU contains four single-speed compressors, totaling eight compressors, which facilitate capacity modulation to match fluctuating thermal loads. Although the compressors vary in size, they are assumed to be identical for modeling purposes. This assumption allows for the application of the calibration procedure as described by Mbaye & Cimmino (2023). In addition to the VRF-HR system, the building incorporates a dedicated outdoor air system (DOAS) that supplies fresh air to the thermal zones, improving indoor air quality and ensuring compliance with ventilation requirements.

The ASHRAE Headquarters Building is highly instrumented, allowing for extensive monitoring of HVAC system performance. The validation of the VRF heat pump model utilizes operational data collected over a two-year period, from July 1, 2011, to June 30, 2013, covering various operational conditions, including seasonal variations and peak load scenarios. The collected data includes indoor and outdoor air

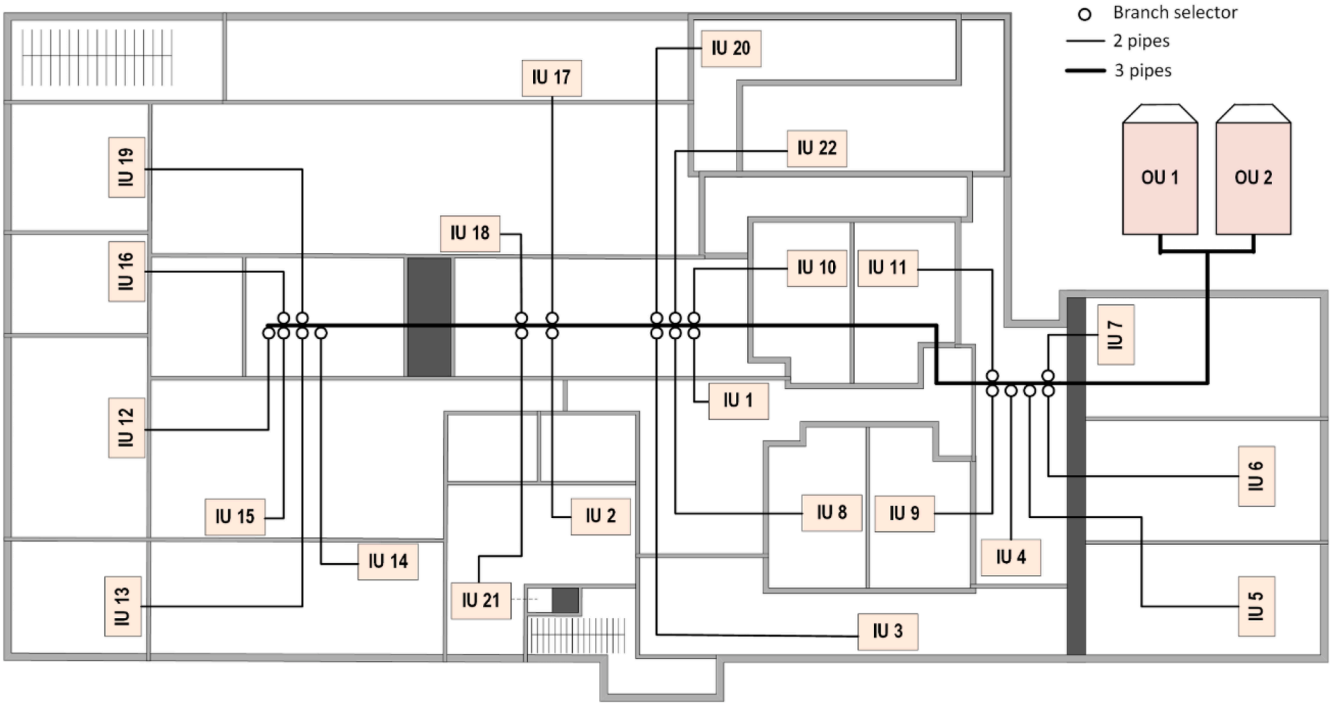

Fig. 3. VRF-HR layout on the first-floor.

temperatures, setpoints, system power consumption, and IU operating statuses.

Different parameters are recorded at varying intervals. Zone temperatures, airflow rates, and discharge air temperatures are logged every 15 minutes, while system operating modes, IU operating status, and occupancy changes are recorded as they occur. The total power consumption of the VRF system and outdoor air temperature are measured at 5-minute intervals. A detailed description of the HVAC system design, control strategies, and performance analysis is available in previous studies by (Southard et al., 2014a, 2014b), offering valuable insights into the design and operation and of the VRF system. Furthermore, comprehensive engineering documentation, including manufacturer operation and installation manuals, are available to support the validation process.

However, some recorded data differ from the inputs required by the VRF-HR model. Return air temperature, a key input, is not directly recorded and is challenging to estimate due to air mixing variations. In certain zones, fresh air is supplied directly from the DOAS, while in others, fresh air from the DOAS mixes with the return air before being supplied to the IUs. To ensure consistency with the available data and following the approach of (Southard et al., 2014b), it is assumed that the return air temperature is equal to the zone air temperature, regardless of the DOAS configuration. Similarly, as no humidity data is recorded, a standard return air relative humidity of 50 % is applied, per ASHRAE Standard 55 recommendations. Uncertainty analysis by Southard et al. (2014b) highlights measurement inaccuracies, including ±0.2 °C for air temperatures, ±11.5 % for airflow rates, and negligible uncertainty for electrical measurements.

5.2. System calibration and controller emulation

5.2.1. Indoor units

The parameters of the ASHRAE VRF system model were determined using manufacturer data. The system consists of 22 indoor units IUs, categorized into seven distinct types, which are anonymized as #1 through #7. Each type underwent a dedicated parameter-estimation procedure. Cooling mode was chosen for calibration as it provides data for both sensible and latent heat transfer. Table 1 lists the corresponding type assignment for all 22 IUs, along with the calibration results. The results include operating mass flow rates and the CVRMSE for sensible and latent capacities, offering a comprehensive evaluation of the model's performance. Figure 4 compares the calibration results from the simulation model with the manufacturer data for both latent and sensible capacities across all IU types. The comparison reveals close alignment between the simulation results and the reference data.

5.2.2. Outdoor unit

The OU model parameters vary based on the operation mode, as described in Section 4.1. Consequently, the OU model is calibrated separately for both heating and cooling modes. For heating-only, heating-dominant, and balanced modes, the VRF-HR model uses parameters calibrated with heating data, where the OU operates as an evaporator. Conversely, for cooling-dominant and cooling-only modes, it uses pa-

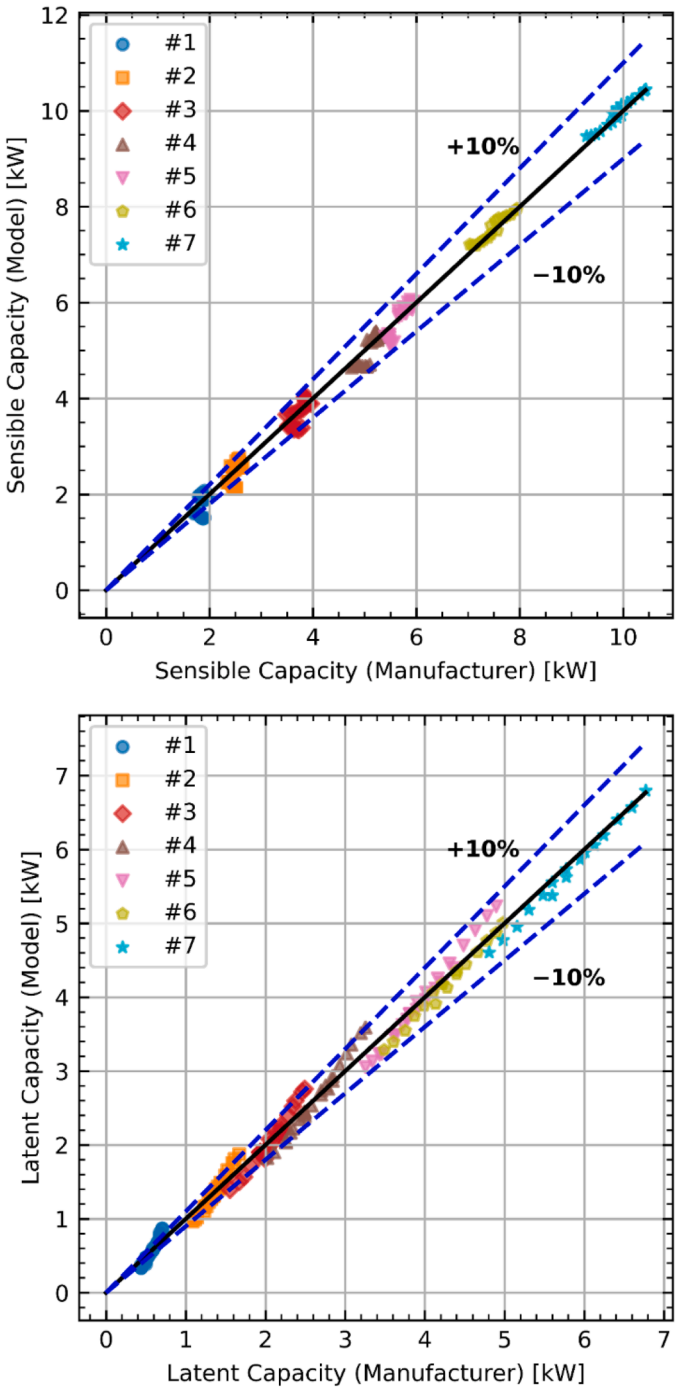

Fig. 4. Comparison between the manufacturer data and the IUs simulation results: latent capacity (top), sensible capacity (bottom).

Table 1
IUs calibration results.

IU Type	Nominal Capacity [kW]	IU #	Nominal Flowrate [l/s]	UA_c [W/K]	UA_{ref} [W/K]	CVRMSE (q_{sen}) [%]	CVRMSE (q_{lat}) [%]
#1	2.05	21	122.7	296	581	4.3	15.4
#2	3.52	1, 2, 8, 9, 10, 11, 13, 16, 22	160.5	303	681	2.9	4.1
#3	5.28	4, 5, 6, 7, 15, 19	250.1	460	1327	3.8	5.7
#4	7.03	12	349.2	620	1161	3.5	6.2
#5	8.80	18, 20	325.6	492	1218	3.3	3.9
#6	10.55	14, 17	481.2	910	2120	3.9	6.8
#7	14.07	3	599.4	1278	1540	3.8	4.3

Table 2
OU parameters obtained after calibration.

Parameters	Condenser	Evaporator
UA_c $[W/K]$	14767	16886
UA_{ref} $[W/K]$	29534	14103
Value per compressor		
$\dot{V}_{nom}$ $[m^3/s]$	17.15e-4	30.40e-4
V_r $[-]$	2.64	2.23
C $[kg/s]$	9.4e-4	7.3e-4
η $[-]$	0.7	0.7
$\dot{W}_{loss}$ $[W]$	6.4	9
ΔT_{sup} $[°C]$	0.5	1

rameters calibrated with cooling data, where the OU functions as a condenser. Table 2 presents the calibrated OU parameters for both evaporator and condenser modes. Figure 5 shows the comparison between the predicted and manufacturer values for total capacity and power input. The calibration results yield CVRMSE values of 1.4 % and 1.8 % for power input and total capacity in condenser mode, and 1.6 % and 3.9 % for evaporator mode, respectively.

5.2.3. Controller tuning

The VRF-HR system controller decision rules are tuned using two methods: manufacturer data and measured operational data from the building's VRF system. The manufacturer data includes combination ratios ranging from 50 % to 130 % for single-mode operation, which are too high to represent scenarios with only one compressor. To address this, artificial data is generated for a 5 % combination ratio to simulate single-compressor operation. This is achieved by selecting each pairing of IU and OU temperature values from the manufacturer dataset, assigning a combination ratio of 5 %, and setting the number of active compressors to one for these conditions. Compressor maps are generated for both cooling and heating modes, with an example for heating mode shown in Figure 6.

The compressor maps for both modes are used to train the decision tree controller model. The manufacturer-tuned controller achieves an overall prediction accuracy of 73 % in heating-only mode and 71 % in cooling-only mode, with detailed performance metrics for each compressor class provided in Table 3. The selection process for compressors in HR mode is further explained in Section 4.1.

Additionally, a measurement-tuned controller is developed using recorded operational data, where compressor mapping is based on VRF power consumption, as VRF capacity data is not available. This method results in an overall prediction accuracy of 68 %, with class-wise performance metrics detailed in Table 4.

5.3. Validation Procedure

The validation of the VRF-HR model involves simulating the system under real operating conditions and comparing its output to measured data and a widely used benchmark model. The simulation spans two periods, each focusing on different aspects of the system's operation and control strategies.

For the first validation period, covering July 1, 2011, to June 30, 2012, the VRF-HR system is simulated using recorded building operating conditions, including all operational modes and varying load conditions. During this phase, a manufacturer-tuned controller is employed and the model's results are compared to measured data. To further evaluate the accuracy of the model itself, independently of the controller performance, results with the best-case controller are also assessed. This best-case controller determines the optimal operation mode and number of compressors at each simulation point to minimize the error between simulated and measured data.

For the second validation period (July 1, 2012 - June 30, 2013), the focus shifts to validating the VRF-HR model specifically in heat recovery

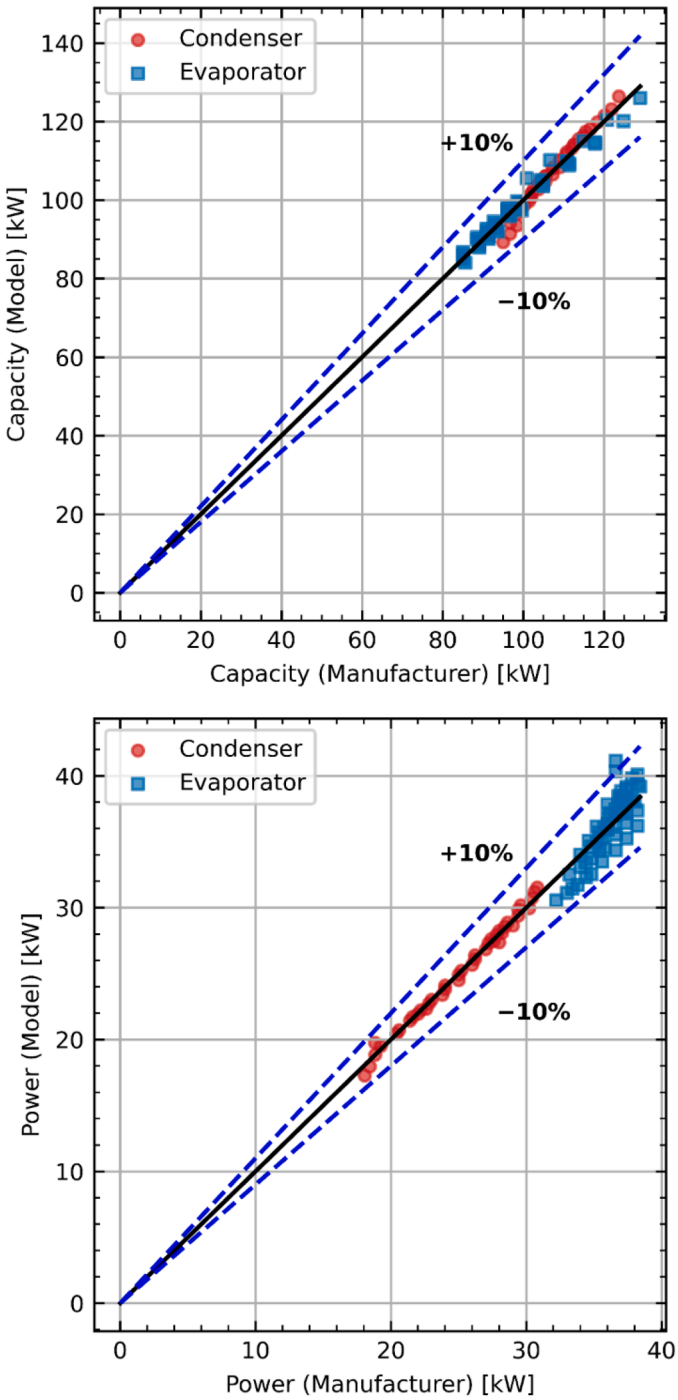

Fig. 5. Comparison of manufacturer data and simulation results for total capacity (top) and power consumption (bottom) in heating and cooling modes.

operation. In addition to the manufacturer-tuned controller, this phase introduces a measurement-tuned controller, trained using data from the first validation period. The results from the VRF-HR model are compared to measured data and the widely used EnergyPlus equation-fit model (VRF-SysCurve) for additional context. The VRF-SysCurve model uses manufacturer performance data for single-mode operation to generate system performance curves. For heat recovery operation, the model applies correction factors – 0.91 for capacity and 1.14 for power consumption – according to EnergyPlus documentation (US Department of Energy, 2024).

The normalized mean bias error (NMBE) and the coefficient of variation of the root mean square error (CVRMSE) are used to quantify

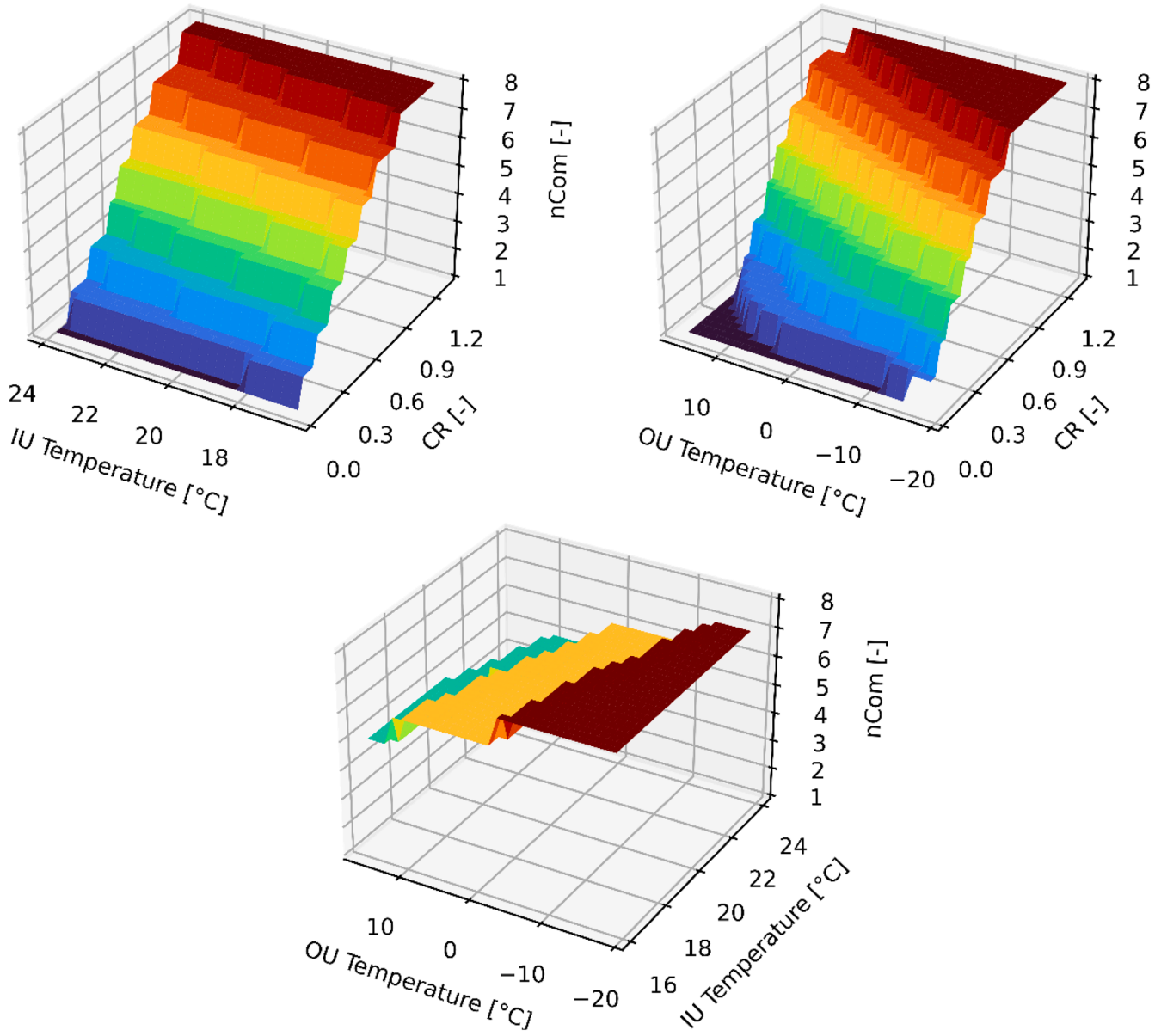

Fig. 6. A compressor map generated using the manufacturer data in heating mode.

discrepancies between simulated and measured data.

$$NMBE = \frac{1}{\overline{m}} \frac{\sum_{i=1}^{n}(m_i - s_i)}{n} \cdot 100(\%) \quad (50)$$

$$CVRMSE = \frac{1}{\overline{m}} \sqrt{\frac{\sum_{i=1}^{n}(m_i - s_i)^2}{n}} \cdot 100(\%) \quad (51)$$

According to ASHRAE Guideline 14 (ASHRAE, 2014), the acceptable limits for hourly data are 30 % for CVRMSE and 10 % for NMBE, while for monthly data, the limits are 15 % for CVRMSE and 5 % for NMBE. These metrics limits serve as benchmarks for assessing the model's accuracy.

6. Results

The validation of the VRF-HR model is conducted by comparing the simulated power consumption with the measured data from the building's first year of operation. Table 5 presents the statistical errors, including CVRMSE, NMBE and relative error. Based on ASHRAE calibration criteria, the manufacturer-tuned VRF-HR model is validated with a CVRMSE of 27.2 %, a NMBE of 6.2 %, and a relative error of 9.5 %. When using the best controller, these results improve significantly, with CVRMSE reduced to 13.1 %, NMBE to 0.1 %, and relative error to 5 %.

Figure 7 illustrates the comparison between simulation results and measured data for a typical week, focusing on power consumption, operation mode, and the number of active compressors. When trained with manufacturer data, the model effectively captures load variations and predicts both system operation and power consumption. However, the comparison between the manufacturer-tuned controller and the optimal controller highlights the significant impact of controller performance. In some instances, inaccuracies in predicting the operation mode or the number of active compressors result in deviations in power consumption.

For the second year of operation, the measured data are compared with the simulation results of three models: the manufacturer-tuned VRF-HR, the measurement-tuned VRF-HR, and the EnergyPlus SysCurve model. As shown in Table 6, both VRF-HR models meet the ASHRAE calibration criteria. The manufacturer-tuned model achieves a

Table 3
Decision tree prediction score for the manufacturer-tuned controller.

Class	Cooling only mode			Heating only mode		
	Precision	Recall	F1-Score	Precision	Recall	F1-Score
1	1	1	1	1	1	1
2	1	0.4	0.57	0.67	0.67	0.67
3	0.76	0.83	0.79	0.69	0.75	0.72
4	0.63	0.8	0.71	0.62	0.47	0.53
5	0.62	0.54	0.58	0.39	0.41	0.4
6	0.43	0.46	0.44	0.53	0.55	0.54
7	0.42	0.28	0.33	0.32	0.41	0.36
8	0.86	0.93	0.9	0.93	0.9	0.91

Table 4
Decision tree prediction score for the measurement-tuned controller.

Class	Precision	Recall	F1-Score
1	0.71	0.82	0.76
2	0.72	0.73	0.72
3	0.68	0.73	0.7
4	0.69	0.69	0.69
5	0.69	0.67	0.68
6	0.63	0.59	0.61
7	0.56	0.47	0.51
8	0.79	0.58	0.67

CVRMSE of 25.3 %, NMBE of 5 %, and a relative error of 7 %, while the measurement-tuned model returns CVRMSE of 29.2 %, NMBE of 5.1 %, and relative error of 7.1 %. In contrast, the SysCurve model exhibits significant errors, with a CVRMSE of 39.9 %, NMBE of 7.8 %, and relative error of 15.5 %. Unexpectedly, the manufacturer-tuned controller outperforms the measurement-tuned controller across all error metrics. This result may be explained by differences in the tuning approach, as the monitored dataset lacks sufficient data for heating-only mode, which could have influenced the accuracy of the measurement-tuned model.

Given that the building is located in Atlanta, USA (IECC climate zone 3A, Mixed-Humid), the VRF system operates under diverse modes throughout the year. Monthly variations in outdoor temperatures lead to a dynamic shift between cooling-only and heat recovery operation modes. As illustrated in Table 7, the system operates almost exclusively in cooling-only mode from June to September (≥85 %), while heat recovery becomes dominant during colder months (October to May), with various sub-modes (cooling-dominant, balanced, or heating-dominant) being triggered. The heat recovery modes are the prevailing operational state for much of the year as they collectively account for 54 % of the total annual operation time.

To evaluate model accuracy under these diverse monthly conditions, the CVRMSE and NMBE metrics were computed for each model across all months. Figure 8 displays these prediction errors. In summer months (June to September), where the operation is primarily cooling-only, all models achieve their highest accuracy, with the manufacturer-tuned model maintaining CVRMSE values below the 30 % threshold and NMBE near 5 %. However, during the shoulder and winter months (October to May), where heat recovery modes are more frequent and dynamic, prediction errors increase. The measurement-tuned model generally remains within the calibration criteria across most months, with only slight exceedances observed in a few cases, such as a CVRMSE above the threshold in April and December, and a peak NMBE of 10.5 % in October. In contrast, the SysCurve model consistently shows higher errors, particularly from October to March, with CVRMSE exceeding 50 % in several instances and NMBE surpassing the 10 % calibration threshold in autumn and winter months.

Table 5
Statistical errors of the first-year results.

	Calibration criteria	VRF-HR (Manufacturer-tuned)	VRF-HR (Best controller)
CVRMSE	30	27.2	13.1
NMBE	10	6.2	0.1
Relative error	-	9.5	5

These results are further supported by analyzing the system's power consumption over a typical week between the winter and shoulder seasons (March 4, 2013 - March 9, 2013), as presented in Figure 9. At the beginning of each day, the system typically operates in single-mode, either cooling-only or heating-only. During these periods, the simulation models closely align with the measured data. However, as the day progresses and heat recovery mode becomes the main operation mode, larger discrepancies appear between the measured and simulated data, particularly for the SysCurve model. Additionally, the results highlight specific instances of significant deviations. For example, on March 8, the measurement-tuned VRF-HR model predicts significantly higher power consumption compared to the measured data, indicating potential limitations in the model controller under certain operating conditions.

The performance of the VRF-HR model is also evaluated by examining key operational parameters and comparing the manufacturer-tuned model results with measured data over a full day of operation. Figure 10 presents the comparison for January 15, 2013, while Figure 11 illustrates the results for February 25, 2013. On January 15, 2013, the system starts operating at 5:30 AM in cooling-only mode. The measured power data indicate a gradual ramp-up, while the simulated power exhibits a step-like behaviour, suggesting discrepancies in how the model represents startup dynamics. Between 6:00 AM and 9:15 AM, the system predominantly operates in balance mode. During this period, the controller input T_{low} exceeds T_{high}, leading to a significant difference in power consumption between the simulation and the measured data. In the afternoon, the system shifts to cooling-dominant mode, with a constant number of indoor units operating in heating. The total nominal cooling capacity suggests that some IUs exhibit frequent on/off cycling, with IU#21 being the primary cycling unit. Despite its relatively small nominal capacity of 2 kW, the cycling of IU#21 impacts the T_{high} control variable, which in turn affects the number of active compressors. As a result, the model's number of compressors alternates between three and four, causing fluctuations in power consumption ranging from 14.5 kW to 10 kW. However, these variations are not observed in the measured power. It is worth noting that IU#21 serves the elevator machine room; a zone with distinct thermal loads and setpoints. Its frequent cycling, though involving a small capacity, has a disproportionate influence on T_{high}, thereby triggering shifts in the control logic.

Beyond the impact of IU cycling on power output, the operation on February 25 provides further insights into the system's dynamic characteristics. While the manufacturer-tuned model generally aligns well with the measured data, discrepancies arise during peak transitions. In several instances during the morning, when the system operates in heating-only mode, some IUs shut off simultaneously. This leads to a sudden drop in the simulated power consumption, directly correlated with a sharp decrease in the combination ratio CR. However, the measured power reacts more gradually to these events, with a delayed response occurring in incremental steps rather than instantaneously. For instance, around 10:10 AM, the CR drops abruptly from 0.79 to 0.25, causing the simulated power to decrease significantly from 21.4 kW to 5.3 kW. In contrast, the measured power follows a more progressive decline, first dropping from 27.6 kW to 19.5 kW, and then further reducing from 19.5 kW to 12.4 kW.

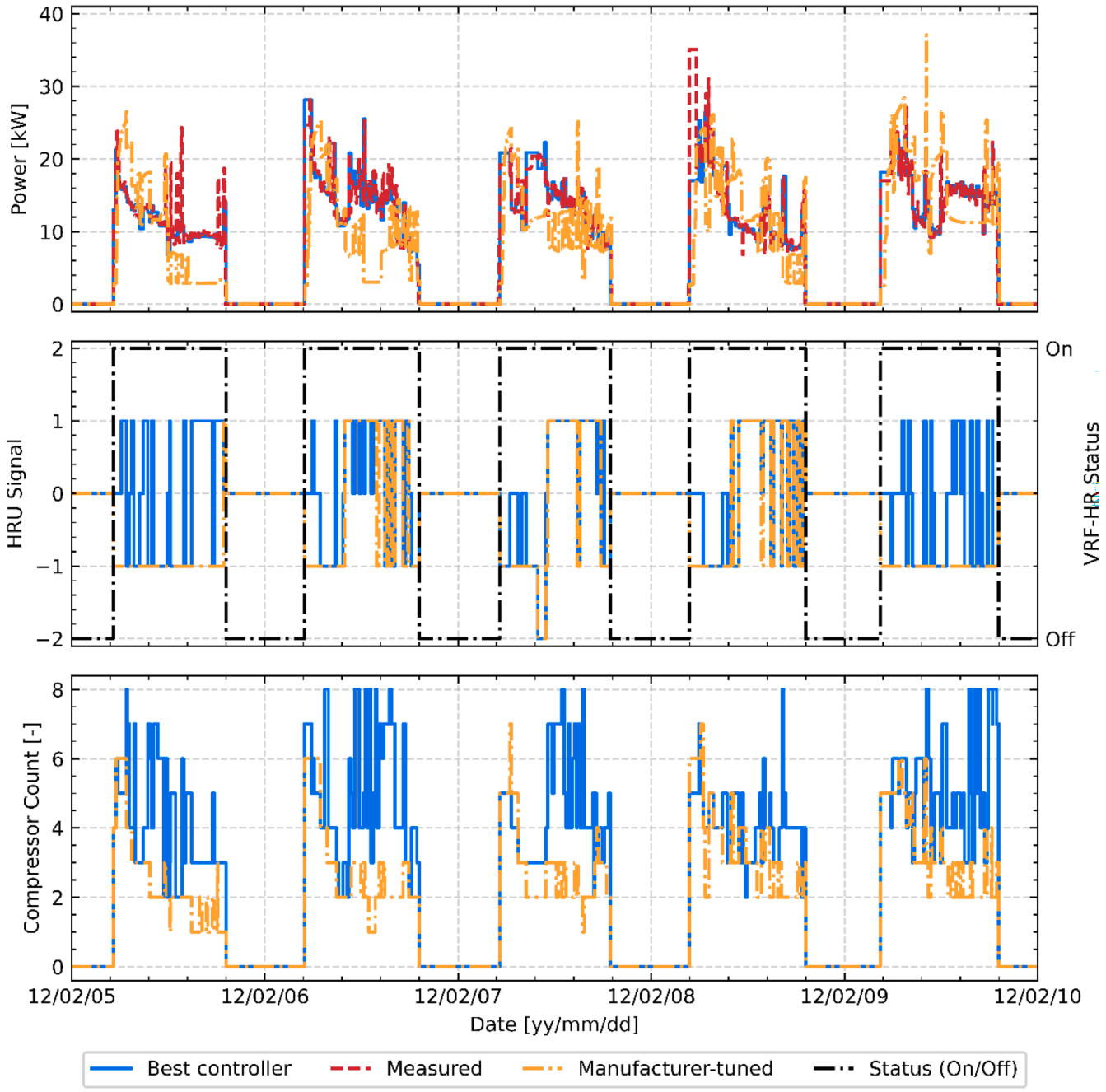

Fig. 7. Comparison results between the simulation and the measurement for a typical week (12/02/05 - 12/02/10): Power consumption (top). Operation mode (middle). Number of working compressors (bottom).

Table 6
Statistical errors of the validation results.

	Calibration criteria	VRF-HR (Manufacturer-tuned)	VRF-HR (Measurement-tuned)	SysCurve Model
CVRMSE	30	25.3	29.2	39.3
NMBE	10	5	5.1	7.8
Relative error	-	7	7.1	15.5

7. Discussion

7.1. Results interpretation

The validation results demonstrate that the VRF-HR model effectively predicts energy consumption and system behavior across various operational modes. It successfully captures power variation trends throughout the year and meets the ASHRAE calibration criteria. However, a closer comparison between the simulated and measured data reveals certain discrepancies that require further analysis. These

Table 7
Monthly frequency of each operation mode.

Operation Mode	HRU Signal	Frequency [%]											
		Jan	Feb	Mar	Apr	May	Jun	Jul	Aug	Sep	Oct	Nov	Dec
Cooling only	2	0	0	2	22	43	85	97	96	100	17	2	1
Cooling dominant	1	18	17	36	50	45	15	2	4	0	57	52	28
Balanced	0	54	23	21	11	8	0	0	0	0	16	18	24
Heating dominant	-1	16	35	22	16	3	0	0	0	0	9	17	30
Heating only	-2	12	25	20	1	0	0	0	0	0	1	11	17

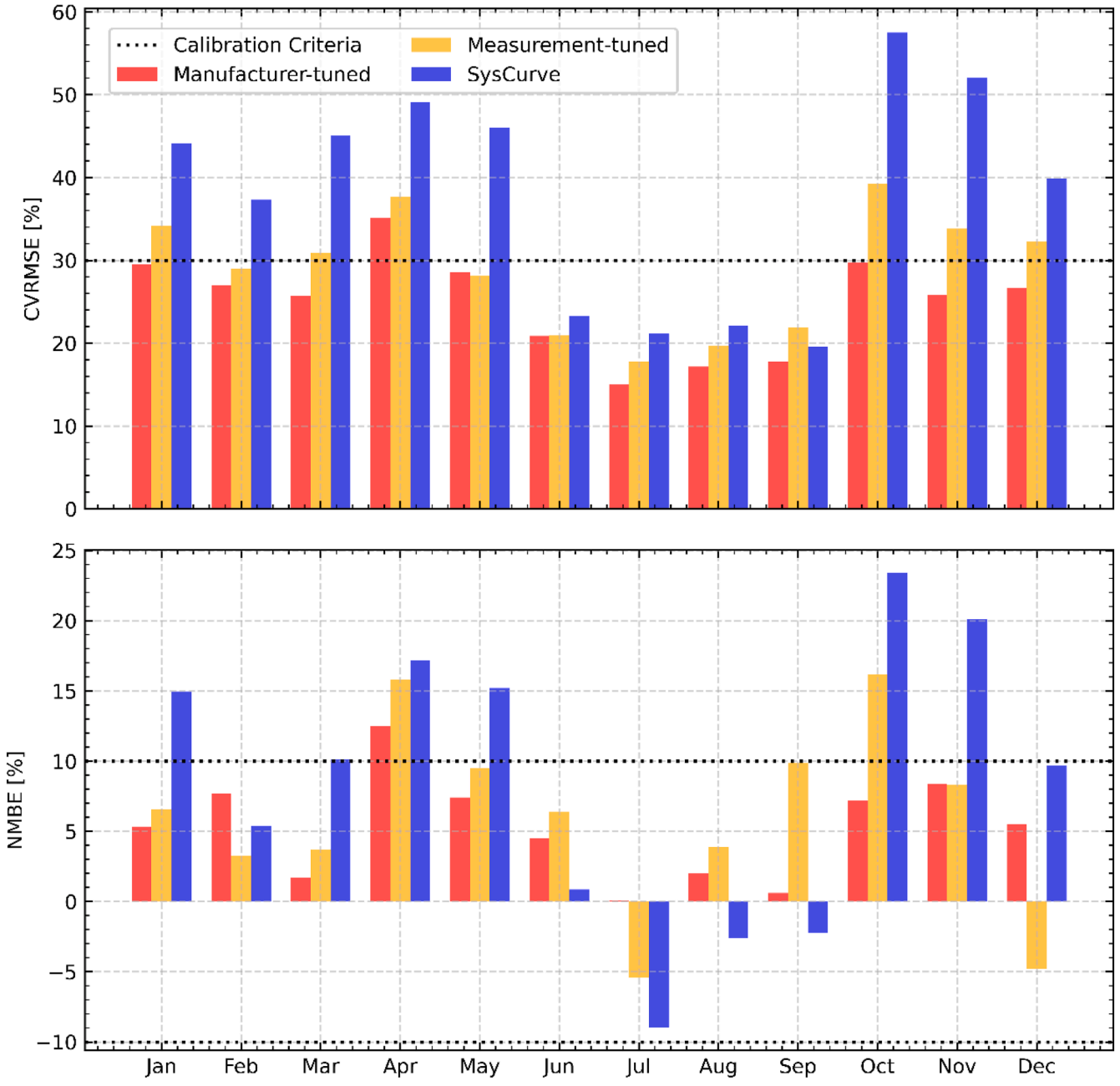

Fig. 8. Monthly prediction errors for each model: CVRMSE (top) and NMBE (bottom).

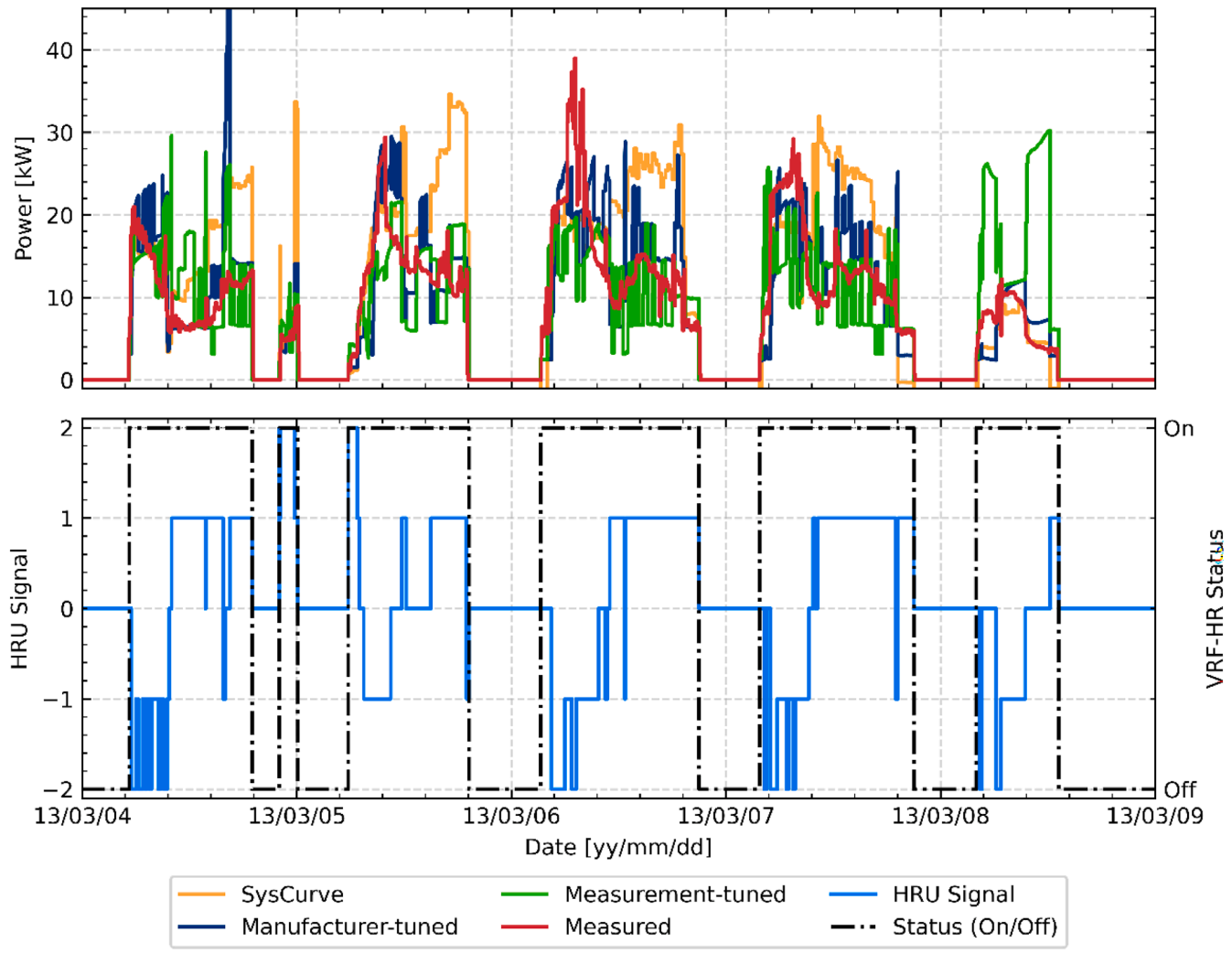

Fig. 9. Comparison of measured data and models results for a typical week (12/03/04 - 13/03/09): Power consumption (top). Operation mode (bottom).

discrepancies can be broadly classified into two categories: those arising from the modeling approach and assumptions and those influenced by external factors and data limitations.

The proposed model does not account for refrigerant piping networks, as it assumes no pressure drop in the refrigerant lines. However, pressure losses significantly impact the capacity of both indoor and outdoor units, which in turn affects compressor power demand and overall system efficiency. This simplification may introduce notable discrepancies, particularly in large-scale VRF systems commonly found in commercial and institutional buildings, where total refrigerant piping length is extensive. Several studies have investigated the impact of refrigerant piping length on system performance. Yan et al. (2012) found that increasing piping length from 2 meters to 20 meters results in a 7.7 % reduction in COP for a 2-IUs VRF system. Similarly, Togashi & Satoh (2021) observed a 10 % decrease in capacity when the piping length increased from 7.5 meters to 100 meters in a 12-IUs VRF system under nominal conditions. Beyond efficiency and capacity losses, piping length also influences system dynamics and transient behavior. The validation results show that the measured power responds more gradually to abrupt changes, whereas the model reacts instantaneously. This discrepancy may be attributed to thermal inertia effects associated with longer refrigerant piping networks. Qiao et al. (2017) noted that indoor unit temperature transients are amplified by a factor of 4.3 when the piping length between the OU and IU increases from 3 meters to 50 meters.

Five operation modes have been identified to characterize the behavior of VRF systems, each represented by a distinct thermodynamic cycle. Therefore, the first step in evaluating system energy consumption under specific operating conditions is to correctly determine the appropriate operation mode corresponding to those conditions. A comparison between the manufacturer-tuned controller and the optimal controller highlighted how inaccuracies in defining the operation mode can lead to significant deviations in power consumption estimation. For the proposed VRF-HR model, this primarily involves accurately setting the boundary conditions for balanced mode in relation to heating-dominant and cooling-dominant modes. As defined in Equation 40, balanced mode activation depends on the relative total capacities of IUs operating in heating and cooling. However, in commercial VRF systems, both balanced mode conditions and the OU HX configuration in this mode are largely dictated by the system's native control logic. Consequently, additional insights into the system's operational characteristics are essential to further refine heat recovery mode modeling and improve the overall accuracy of the VRF-HR model.

The capacity controller relies on two key input temperatures: T_{low} and T_{high}, which are defined as the lowest return air temperature among all evaporators and the highest return air temperature among all condensers, respectively. While this definition aligns with the proposed thermodynamic cycles, it introduces inaccuracies under certain conditions. As shown in Figure 10, instances may arise during heat recovery mode where T_{low} exceeds T_{high}, creating an inconsistency in system

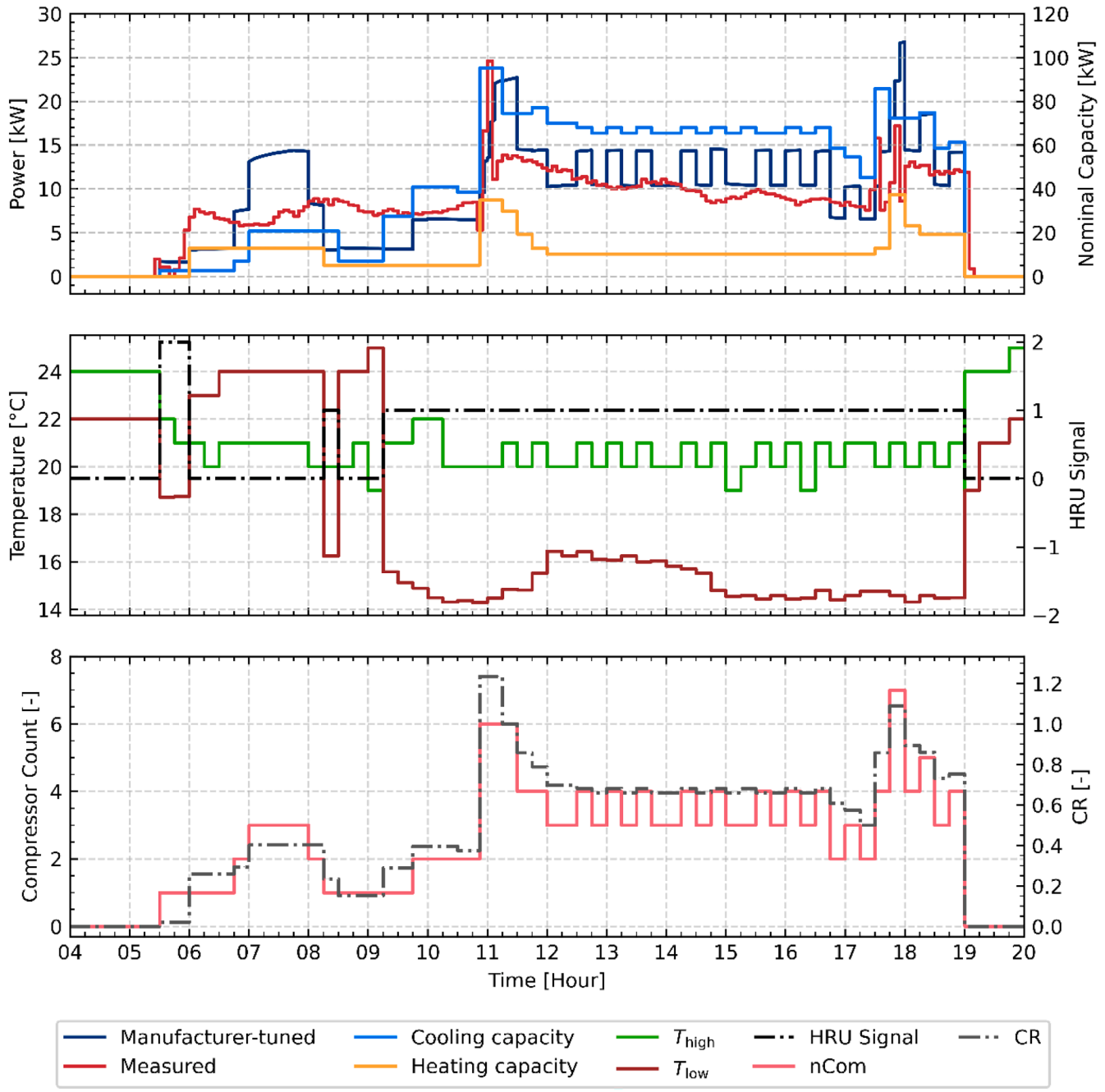

Fig. 10. VRF-HR model operational characteristics for a typical day (January 15, 2013): Power and capacity (top). Temperatures and operation mode (middle). Number of working compressors and combination ratio (bottom).

behavior. Additionally, when an IU with an extreme return air temperature (either the lowest or highest) is turned on or cycling, it immediately becomes the defining temperature for the capacity controller. This abrupt change influences the number of working compressors, leading to power consumption variations. The measured power in those conditions indicate that, to better reflect the overall system state, the temperature selection process within the controller shouldn't be dominated by a single IU at any given moment.

When comparing the simulation results between the manufacturer-tuned controller and the measurement-tuned controller, one might expect the measurement-tuned controller to yield more accurate results since it incorporates operational data from the actual system. However, the results indicate otherwise, as the manufacturer-tuned controller achieves lower CVRMSE and NMBE values, particularly during heat recovery mode operation. This discrepancy can be attributed to differences in the tuning approach used for the two controllers. The controller model is designed to be trained with data in single-mode operation (i.e., heating-only and cooling-only) to determine the number of active compressors. Once this baseline is established, a selection process for working compressors in heat recovery mode is implemented. Conversely, the measured data set includes cooling-only operation but lacks relevant heating-only data, as there is no full day where the system operates exclusively in heating mode. Consequently, the measurement-tuned controller incorporates operation mode as an additional input, alongside temperature and combination ratio. However, since operation mode is not directly recorded, the model's predicted operation mode is used instead. The challenge arises from the fact that the mode predicted by the model may not always align with the actual system's operating

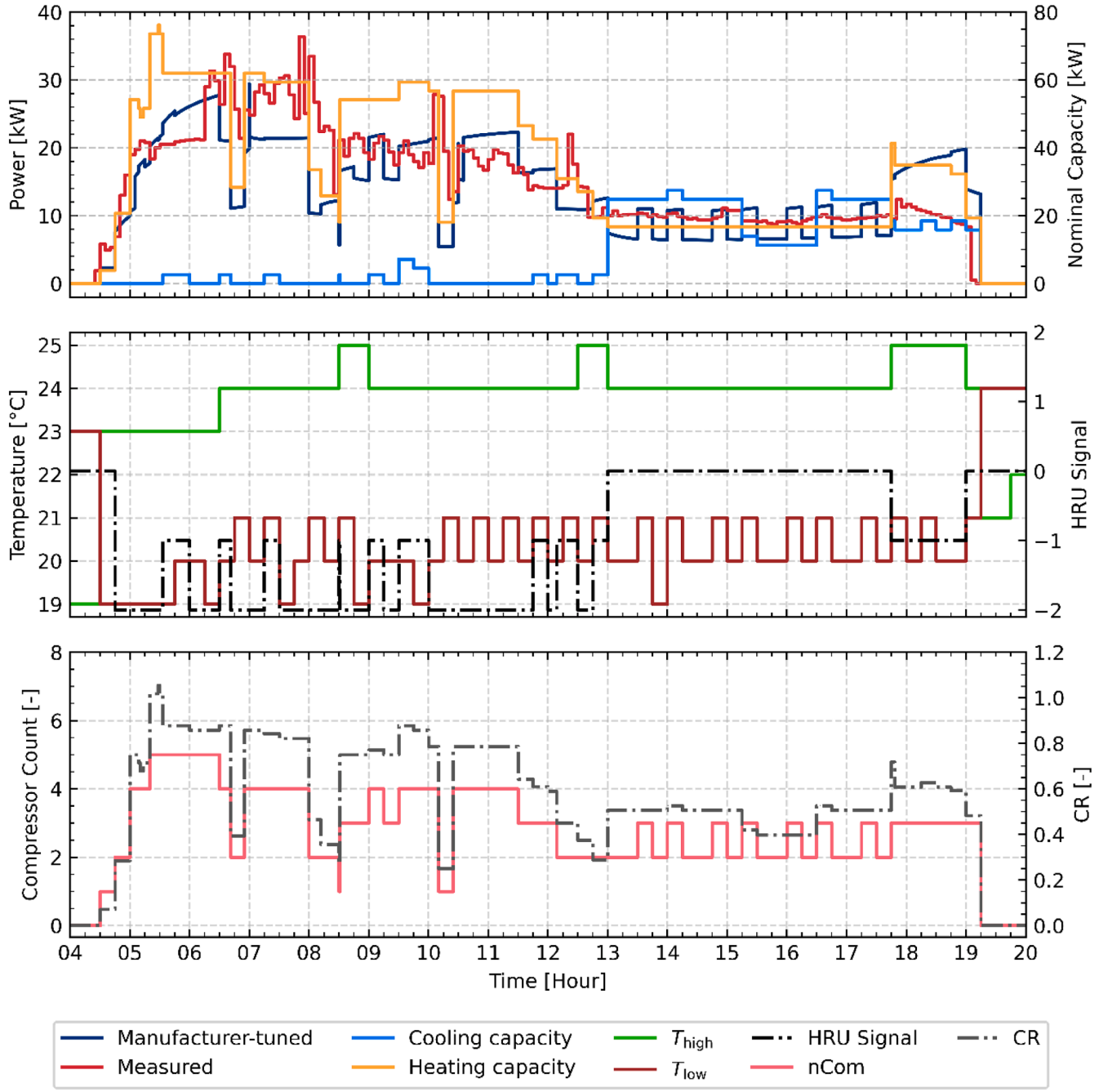

Fig. 11. VRF-HR model operational characteristics for a typical day (February 25, 2013): Power and capacity (top). Temperatures and operation mode (middle). Number of working compressors and combination ratio (bottom).

mode, as the native control logic remains unknown. This introduces additional inaccuracies in the measurement-tuned controller's ability to correctly determine the number of active compressors, ultimately leading to higher errors in power consumption predictions compared to the manufacturer-tuned model.

Beyond the modeling approach and assumptions, some of the discrepancies between measured and simulated data may also stem from limitations in the collected data. One key factor is the lack of recorded mixed air relative humidity, which is instead assumed to be constant at 50 %. This assumption can introduce errors in power consumption estimates, as higher relative humidity increases power demand due to additional latent cooling loads. Another data limitation is the return air temperature estimation for certain IUs. Since actual return air temperatures are not recorded, they are approximated as equal to the zone temperature. However, this approximation may significantly impact power consumption predictions, as it directly affects the controller input temperature, which in turn influences the number of active compressors. The effects of humidity and temperature variations on system power consumption in cooling-only mode have been evaluated in previous studies (Mbaye & Cimmino, 2023). Findings indicate that when all 22 IUs are operational, with T_{low} at 20 °C and T_{high} at 30 °C, the simulated power of the manufacturer-tuned model varies by 13.4 % as relative humidity fluctuates from 0 % to 100 %. Furthermore, under similar conditions, when T_{high} remains at 30 °C and return air humidity is 50 %, the simulated power decreases by 7.7 % when T_{low} drops from 20 °C to 15 °C.

The VRF system's operational parameters are recorded at different time intervals, which introduces a time lag between cause and effect in

the measured data. Specifically, temperature readings are recorded every 15 minutes, power consumption every 5 minutes, and indoor IUs operating status is logged in real-time as changes occur. Due to these asynchronous recording intervals, a change, for example, in the combination ratio may only be reflected in the measured power consumption data up to 5 minutes later. Similarly, fluctuations in power consumption caused by temperature variations may appear 15 minutes before the corresponding temperature change is recorded. This inherent time delay in the measured data contrasts with the simulation, where power consumption is instantly affected by input changes without any recording delay. As a result, this temporal misalignment between measured and simulated data significantly impacts statistical error metrics, particularly the CVRMSE. Since CVRMSE is sensitive to point-by-point deviations, any misalignment amplifies apparent discrepancies even when the model accurately predicts overall trends. The impact becomes more pronounced as the number of data points increases. For instance, the dataset for the second validation period includes over 312,000 data points, meaning even minor delays in measured responses can lead to inflated statistical errors, making the model appear less accurate than it actually is.

7.2. Limitations and Future work

The VRF-HR model has demonstrated its ability to accurately predict energy consumption in large VRF systems operating in both single-mode and heat recovery mode, with errors falling within ASHRAE calibration limits. However, the model exhibits limitations in capturing the dynamic behavior of VRF systems, which is crucial for applications such as demand response, where daily peak power consumption must be assessed, or for control strategy implementation, where precise dynamic characteristics are required. These limitations present opportunities for improvement and avenues for further research.

One key area for improvement is the implementation of pressure drop calculations associated with the refrigerant piping network to enhance model accuracy. Since the VRF-HR model relies on manufacturer data for parameter estimation and controller emulation, a similar data-driven approach can be applied to incorporate pressure drop effects. Manufacturers typically provide capacity correction factors as a function of pipe length and height differences between IUs and OU, often formatted as Abaqus tables or empirical correction curves. Future studies could integrate these correction factors into the VRF-HR model to better account for the impact of refrigerant pressure losses on system performance.

Furthermore, the accuracy of the VRF-HR model is closely linked to its ability to predict the number of active compressors under partial load operation. The decision tree algorithm was selected due to its ability in handling classification problems and its suitability for Boolean logic implementation. However, the current controller model achieves a prediction accuracy of approximately 70 %, indicating potential for improvement. To enhance compressor prediction accuracy, two key strategies could be pursued. First, a more comprehensive onsite dataset could be collected to improve the training process and ensure better generalization across various operating conditions. Second, alternative machine learning methods could be explored to optimize compressor selection. One promising approach is ensemble learning, which involves training multiple machine learning models and combining their outputs to produce a refined prediction (Sagi & Rokach, 2018). Konhäuser et al. (2022) have shown that ensemble learning techniques can significantly improve BEPS models by reducing overfitting and enhancing model robustness. Another advanced approach is hybrid machine learning models, where multiple sub-models are trained, each focusing on a specific characteristic of the system. In the context of VRF systems, hybrid models that integrate data partitioning techniques, Back Propagation Neural Networks (BPNN), and Swarm Intelligence algorithms have been found to outperform single BPNN models in predicting VRF system energy consumption (He et al., 2023).

8. Conclusion

This study presents the development and validation of a new Variable Refrigerant Flow (VRF) heat pump model designed for the simulation of systems operating in both single-mode and heat recovery mode. The model is tailored for multi-year simulations of large-scale systems, making it particularly suitable for commercial and institutional buildings. The proposed modular and flexible modeling approach integrates physics-based component models for indoor units (IUs), outdoor units (OUs), and multiple single-speed compressors. A heat recovery unit (HRU) model is also incorporated, featuring five distinct operational modes, each following a specific vapor compression cycle. The model parameters are determined through a parameter-estimation procedure that leverages manufacturer performance data. Additionally, a data-driven capacity control strategy, based on machine learning techniques, is implemented to dynamically select the optimal number of active compressors based on real-time operational conditions. This approach allows the model to accurately represent commercial VRF systems without requiring detailed knowledge of their proprietary control algorithms.

The validation of the VRF heat recovery (VRF-HR) model, implemented in Modelica, is conducted using two years of real-world operational data from a large-scale VRF system serving the first floor of the former ASHRAE Headquarters Building in Atlanta. The system consists of 22 indoor units, 2 outdoor units, and 8 compressors, operating under various conditions in both single-mode and heat recovery mode. The results demonstrate that the manufacturer-tuned model effectively predicts total energy consumption over an entire year, achieving a relative error of 9.5 %, an NMBE of 6.2 %, and a CVRMSE of 27.2 % when compared to measured data for the first year of validation. For the second year, the model achieves a CVRMSE of 25.3 %, an NMBE of 5 %, and a relative error of 7 %, further confirming its validation based on the ASHRAE calibration criteria.

Several enhancements are proposed to further refine model accuracy and applicability. First, incorporating pressure drop calculations associated with refrigerant piping length would improve predictions of system energy consumption. Second, advancing the control strategy by leveraging ensemble learning and hybrid machine learning techniques could enhance compressor selection accuracy. Overall, this study provides a robust foundation for advancing VRF-HR modeling, bridging the gap between physics-based and data-driven approaches.

CRediT authorship contribution statement

Aziz Mbaye: Writing – original draft, Visualization, Validation, Methodology, Investigation, Formal analysis. **Massimo Cimmino:** Writing – review & editing, Supervision, Conceptualization.

Declaration of competing interest

The authors declare that they have no known competing financial interests or personal relationships that could have appeared to influence the work reported in this paper.

The author is an Editorial Board Member/Editor-in-Chief/Associate Editor/Guest Editor for this journal and was not involved in the editorial review or the decision to publish this article.

Acknowledgment

The authors acknowledge the support of the Natural Sciences and Engineering Research Council of Canada (NSERC), [funding reference number RGPIN-2018-04471]. The authors also acknowledge the support of the NSERC, the Trottier Energy Institute and Hydro-Québec for scholarships awarded to the first author. This study leveraged measured data kindly provided by Dr. Jeffrey Spitler and Laura Southard, for which the authors are deeply appreciative.

References

ASHRAE. (2014). Measurement of Energy and Demand Savings *ASHRAE Guideline 14*.

ASHRAE. (2020). *ASHRAE Handbook—HVAC Systems and Equipment*.

Chen, Y., Halm, N., Groll, E.A., Braun, J.E., 2000. A Comprehensive Model of Scroll Compressors, Part II: Overall Scroll Compressor Modeling. In: Paper presented at the International Compressor Engineering Conference at Purdue Purdue University, West Lafayette, IN.

Dong, L., Li, Y., House, J.M., Salsbury, T.I., 2017. Mode switching control for a multi-functional variable refrigerant flow system. Science and Technology for the Built Environment 24 (4), 418–434. https://doi.org/10.1080/23744731.2017.1406275.

Dong, L., Li, Y., Salsbury, T.I., House, J.M., Wu, Z., 2017. Multi-variable extremum seeking control for a multi-functional variable refrigerant flow system. Science and Technology for the Built Environment 24 (4), 382–395. https://doi.org/10.1080/23744731.2017.1393257.

He, Y., Gong, Q., Zhou, Z., Chen, H., 2023. Development of a hybrid VRF system energy consumption prediction model based on data partitioning and swarm intelligence algorithm. Journal of Building Engineering 74, 106868. https://doi.org/10.1016/j.jobe.2023.106868.

Hong, T., Sun, K., Zhang, R., Hinokuma, R., Kasahara, S., Yura, Y., 2016. Development and validation of a new variable refrigerant flow system model in EnergyPlus. Energy and Build. 117, 399–411. https://doi.org/10.1016/j.enbuild.2015.09.023.

Hunt, W., Upadhye, H., Domitrovic, R., Delany, P., Tsan, B., Vowles, M., 2012. Variable Refrigerant Flow-Heat Recovery Performance Characterization. Paper presented at the. In: 2012 ACEEE Summer Study on Energy Efficiency in Buildings.

Jin, H., 2002. Parameter estimation based models of water source heat pumps. Oklahoma State University. PhD Thesis.

Jin, H., Spitler, J.D., 2002. A parameter estimation based model of water-to-water heat pumps for use in energy calculation programs. ASHRAE Transactions 108 (Part 1), 3–17.

Kim, D., Cox, S.J., Cho, H., Im, P., 2018. Model calibration of a variable refrigerant flow system with a dedicated outdoor air system: A case study. Energy and Buildings 158, 884–896. https://doi.org/10.1016/j.enbuild.2017.10.049.

Konhäuser, K., Wenninger, S., Werner, T., Wiethe, C., 2022. Leveraging advanced ensemble models to increase building energy performance prediction accuracy in the residential building sector. Energy and Buildings 269, 112242. https://doi.org/10.1016/j.enbuild.2022.112242.

Li, X., Wu, W., Yu, C.W.F., 2014. Energy demand for hot water supply for indoor environments: Problems and perspectives. Indoor and Built Environment 24 (1), 5–10. https://doi.org/10.1177/1420326×14564285.

Li, Y.M., Wu, J.Y., 2010. Energy simulation and analysis of the heat recovery variable refrigerant flow system in winter. Energy and Buildings 42 (7), 1093–1099. https://doi.org/10.1016/j.enbuild.2010.01.023.

Lin, X., Lee, H., Hwang, Y., Radermacher, R., 2015. A review of recent development in variable refrigerant flow systems. Science and Technology for the Built Environment 21 (7), 917–933. https://doi.org/10.1080/23744731.2015.1071987.

Lin, X., Lee, H., Hwang, Y., Radermacher, R., Kim, B., 2016. A New Variable Refrigerant Flow System Simulation Approach in EnergyPlus. International Journal of Air-Conditioning and Refrigeration 24 (01), 1650001. https://doi.org/10.1142/s2010132516500012.

Lin, X., Lee, H., Hwang, Y., Radermacher, R., Oh, S., 2015. Field test of multi-functional variable refrigerant flow system. Science and Technology for the Built Environment 21 (5), 648–657. https://doi.org/10.1080/23744731.2015.1047720.

Mbaye, A., Cimmino, M., 2023. Variable refrigerant flow heat pump model with estimated parameters and emulated controller based on manufacturer data. Science and Technology for the Built Environment 1–18. https://doi.org/10.1080/23744731.2023.2279469.

McElgin, J., Wiley, D.C., 1940. Calculation of coil surface areas for air cooling and dehumidification. Heating, Piping and Air Conditioning 12 (1), 195–201.

Oh, K., Kim, E.-J., 2024. Predicting the energy consumption of a VRF heat pump using manufacturer performance data and limited experimentation for dynamic data collection. Energy and Buildings 303, 113798. https://doi.org/10.1016/j.enbuild.2023.113798.

Pachano, J.E., Peppas, A., Bandera, C.F., 2022. Seasonal adaptation of VRF HVAC model calibration process to a mediterranean climate. Energy and Buildings 261, 111941. https://doi.org/10.1016/j.enbuild.2022.111941.

Qiao, H., Laughman, C.R., Burns, D.J., Bortoff, S.A., 2017. In: *Dynamic Characteristics of an R410a Multi-split Variable Refrigerant Flow Air-conditioning System* Paper presented at the 12th IEA Heat Pump Conference, Rotterdam.

Raustad, R., 2013. A Variable Refrigerant Flow Heat Pump Computer Model in EnergyPlus. Ashrae Transactions 119 (Pt 1), 299–308. *2013, Vol 119*.

Reddy, T.A., 2006. Literature review on calibration of building energy simulation programs: Uses, problems, procedures, uncertainty, and tools. Ashrae Transactions 112 (Pt 1), 226–240. *2006, Vol 112*.

Sagi, O., Rokach, L., 2018. Ensemble learning: A survey. Wiley Interdisciplinary Reviews-Data Mining and Knowledge Discovery 8 (4).

Sharma, C., Raustad, R., 2013. Compare Energy Use in Variable Refrigerant Flow Heat Pumps Field Demonstration and Computer Model. Ashrae Journal 119 (2), 1–8.

Southard, L., Liu, X., Spitler, J., 2014a. Performance of HVAC Systems at ASHRAE HQ Part.1. Ashrae Journal 56 (9), 14–22.

Southard, L., Liu, X., Spitler, J., 2014b. Performance of HVAC Systems at ASHRAE HQ Part.2. Ashrae Journal 56 (12), 12–23.

Sun, H., Ding, G., Hu, H., Ren, T., Xia, G., Wu, G., 2017. A general simulation model for variable refrigerant flow multi-split air conditioning system based on graph theory. International Journal of Refrigeration 82, 22–35. https://doi.org/10.1016/j.ijrefrig.2017.07.003.

Thornton, B., & Wagner, A. (2012). *Variable Refrigerant Flow Systems*. Retrieved from.

Togashi, E., Satoh, M., 2021. Development of variable refrigerant flow heat-pump model for annual-energy simulation. Journal of Building Performance Simulation 14 (5), 554–585. https://doi.org/10.1080/19401493.2021.1986573.

Torregrosa-Jaime, B., Martinez, P.J., Gonzalez, B., Paya-Ballester, G., 2019. Modelling of a variable refrigerant flow system in energyplus for building energy simulation in an open building information modelling environment. Energies 12 (1). https://doi.org/10.3390/en12010022.

US Department of Energy. (2024). *EnergyPlus™ Version 24.1.0 Documentation: Engineering Reference*. Washington, DC.

Wan, H., Cao, T., Hwang, Y., Oh, S., 2020. A review of recent advancements of variable refrigerant flow air-conditioning systems. Applied Thermal Engineering 169, 114893. https://doi.org/10.1016/j.applthermaleng.2019.114893.

Wang, J., Lu, X., Adetola, V., Louie, E., 2024. Modeling Variable Refrigerant Flow (VRF) systems in building applications: A comprehensive review. Energy and Buildings 311, 114128. https://doi.org/10.1016/j.enbuild.2024.114128.

Wetter, M., Fuchs, M., Grozman, P., Helsen, L., Jorissen, F., Müller, D., Thorade, M., 2015. IEA EBC Annex 60 Modelica Library - An international collaboration to develop a free open-source model library for buildings and community energy systems. Paper presented at the. In: International Conference of the International Buildings Performance Simulation Association, Hyderabad.

Winandy, E., Saavedra, C., Lebrun, J., 2002. Experimental analysis and simplified modelling of a hermetic scroll refrigeration compressor. Applied Thermal Engineering 22 (2), 107–120. https://doi.org/10.1016/s1359-4311(01)00083-7.

Wu, C., Xingxi, Z., Shiming, D., 2005. Development of control method and dynamic model for multi-evaporator air conditioners (MEAC). Energy Conversion and Management 46 (3), 451–465. https://doi.org/10.1016/j.enconman.2004.03.004.

Yan, P., Xiangguo, X., Liang, X., Shiming, D., 2012. A modeling study on the effects of refrigerant pipeline length on the operational performance of a dual-evaporator air conditioning system. Applied Thermal Engineering 39, 15–25. https://doi.org/10.1016/j.applthermaleng.2012.01.006.

Yun, G.Y., Song, K., 2017. Development of an automatic calibration method of a VRF energy model for the design of energy efficient buildings. Energy and Buildings 135, 156–165. https://doi.org/10.1016/j.enbuild.2016.11.060.

Zhang, R., Sun, K., Hong, T., Yura, Y., Hinokuma, R., 2018. A novel Variable Refrigerant Flow (VRF) heat recovery system model: Development and validation. Energy and Buildings 168, 399–412. https://doi.org/10.1016/j.enbuild.2018.03.028.

Zhou, Y.P., Wu, J.Y., Wang, R.Z., Shiochi, S., 2007. Energy simulation in the variable refrigerant flow air-conditioning system under cooling conditions. Energy and Buildings 39 (2), 212–220. https://doi.org/10.1016/j.enbuild.2006.06.005.

Zhou, Y.P., Wu, J.Y., Wang, R.Z., Shiochi, S., Li, Y.M., 2008. Simulation and experimental validation of the variable-refrigerant-volume (VRV) air-conditioning system in EnergyPlus. Energy and Buildings 40 (6), 1041–1047. https://doi.org/10.1016/j.enbuild.2007.04.025.

Zhu, Y., Jin, X., Du, Z., Fan, B., Fu, S., 2013. Generic simulation model of multi-evaporator variable refrigerant flow air conditioning system for control analysis. International Journal of Refrigeration 36 (6), 1602–1615. https://doi.org/10.1016/j.ijrefrig.2013.04.019.